atmosphere

MDPI

Review

Review: The Use of Real-Time Fluorescence Instrumentation to Monitor Ambient Primary Biological Aerosol Particles (PBAP)

Mehael J. Fennelly [1,2,3], Gavin Sewell [4], Michael B. Prentice [2,5], David J. O'Connor [4,*] and John R. Sodeau [1,3]

1 Department of Chemistry, University College Cork, T12 YN60 Cork, Ireland; 116224792@umail.ucc.ie (M.J.F.); j.sodeau@ucc.ie (J.R.S.)
2 Department of Microbiology, University College Cork, T12 YN60 Cork, Ireland; M.Prentice@ucc.ie
3 Environmental Research Institute, University College Cork, T23 E4PW Cork, Ireland
4 School of Chemical and Pharmaceutical Sciences, Dublin Institute of Technology, Kevin Street, Dublin 8, Ireland; 060277@dit.ie
5 APC Microbiome Institute, University College Cork, T12 YN60 Cork, Ireland
* Correspondence: david.x.oconnor@dit.ie

Received: 14 October 2017; Accepted: 12 December 2017; Published: 21 December 2017

Abstract: Primary biological aerosol particles (PBAP) encompass many particle types that are derived from several biological kingdoms. These aerosol particles can be composed of both whole living units such as pollen, bacteria, and fungi, as well as from mechanically formed particles, such as plant debris. They constitute a significant proportion of the overall atmospheric particle load and have been linked with adverse health issues and climatic effects on the environment. Traditional methods for their analysis have focused on the direct capture of PBAP before subsequent laboratory analysis. These analysis types have generally relied on direct optical microscopy or incubation on agar plates, followed by time-consuming microbiological investigation. In an effort to address some of these deficits, real-time fluorescence monitors have come to prominence in the analysis of PBAP. These instruments offer significant advantages over traditional methods, including the measurement of concentrations, as well as the potential to simultaneously identify individual analyte particles in real-time. Due to the automated nature of these measurements, large data sets can be collected and analyzed with relative ease. This review seeks to highlight and discuss the extensive literature pertaining to the most commonly used commercially available real-time fluorescence monitors (WIBS, UV-APS and BioScout). It discusses the instruments operating principles, their limitations and advantages, and the various environments in which they have been deployed. The review provides a detailed examination of the ambient fluorescent aerosol particle concentration profiles that are obtained by these studies, along with the various strategies adopted by researchers to analyze the substantial data sets the instruments generate. Finally, a brief reflection is presented on the role that future instrumentation may provide in revolutionizing this area of atmospheric research.

Keywords: PBAP; WIBS; UV-APS; BioScout; fluorescence; real-time; bioaerosols

1. Introduction

Aerosols constitute a significant portion of the Earth's atmosphere. This ubiquity within the atmosphere results in substantial ecological, health, and climatic effects to the planet. Aerosols are defined as suspensions of liquid or solid particles in a gas that possess a broad range of physical diameters, which span from the ultrafine (i.e., <100 nm) to the super coarse >10 μm [1–3]. Primary Biological Aerosol Particles (PBAP) make up a substantial fraction of the total aerosol, and encompass particle types such as pollen, fungal spores, and bacterial cells/agglomerates amongst many others.

The study of PBAP has recently undergone significant growth, with increasing research interest focused on determining the overall concentrations, as well as the identification of ambient species. This increased effort stems from the ever accumulating evidence that certain biological particles are linked to detrimental health conditions [4]. High concentrations of both fungal and bacterial spores have been implicated in numerous diseases and health problems for humans, flora, and fauna. For example, respiratory problems, such as chronic obstructive pulmonary disease (COPD) and farmers' lung have been conclusively linked to aeroallergen interactions within both humans and animals [5]. Several spore forming fungal species, including *Aspergillus fumigatus*, *Aspergillus flavus*, *Aspergillus parasiticus*, and *Alternaria alternata* are also known to produce mycotoxins [6]. This fact is important because the inhalation of mycotoxins has been linked with diseases such as cancer, as well as renal failure [7]. Likewise, the long-term exposure to fine particulate matter (<2.5 μm) by inhalation and deposition in the respiratory tract, has been determined to be deleterious to public health and leads to increased risk of morbidity and mortality of sensitive groups [8–11].

Primary biological aerosol particles have the potential to affect the radiative balance of the planet. They can do this by directly scattering light, but also by acting as "seeds" for the growth of ice nuclei (IN) in cloud formation [12]. Ice nucleating particles (INPs) are generally thought to represent a small subsection of total ambient particles. INPs have surface characteristics that allow for them to cause freezing at warmer temperatures or lower supersaturations (heterogeneous nucleation) than would normally be seen via homogenous nucleation [13,14]. While some modeling studies have pointed towards PBAP as being unimportant for ice nucleation on a global and annual scale, this may not be the case on regional and seasonal scales, especially if high levels of biological particles are present and other types of INPs are low [14–16]. Based on these observations, real-time bioaerosol sensors have begun to be utilized in an attempt to identify the particular biological particles that are associated with ice nucleation within the atmosphere along with the meteorological conditions that enhance their propensity to induce ice nucleation.

Traditionally, PBAP numbers and types were determined by use of impaction instrumentation, whereby particles are sampled onto a suitable substrate before counting and identification. The analysis methods commonly adopted include optical microscopy or agar plate culturing [17–20]. More recently, the use of fluorescence detection in the real-time monitoring of ambient particles has grown in popularity, and has been utilized in several widely differing environments [21–23]. The popularity of these instruments have surged for several reasons, including: (i) Superior time resolution (millisecond) in comparison to most traditional techniques which sample over days or weeks; (ii) The techniques are non-destructive; and, (iii) The processing requires few consumables for operation, and generally does not require an extensively trained operator to extract the data when compared to some of the more subjective conventional methods. It should be noted that while the instruments under review were designed for the detection of primary biological aerosol particles (PBAP), the presence of interfering non-biological fluorescent particles often contributes to the total fluorescent count. The concentration values are therefore generally reported as fluorescent aerosol particles (FAP) to reflect the contribution of this unknown component.

Based on the myriad potential advantages that are offered by fluorescent detection over more traditional particle monitoring and their extensive utilization across diverse research disciplines, a thorough review discussion of the three most utilized commercially available real-time fluorescent instruments is now warranted. This work will initially give a brief introduction to the fluorescent nature of biological particles and their role as potential interferents, followed by a discussion and comparison of the most commonly employed instrumentation, with a particular focus on the results that are gleaned from diverse field deployments. Finally some thoughts on the future directions that instrumentation is taking will be offered. This work aims to collate the extensive work that is performed in this area, while also highlighting avenues of exploration where more intense research effort may prove useful.

1.1. PBAP Fluorescence:

Intrinsic fluorescence (also known as autofluorescence) of PBAP is caused by the presence of naturally occurring fluorescent molecular components (bio-fluorophores) within the sampled particle. Extensive reviews on the subject are already available [24–26], thus only a brief overview of them will be given here and can be seen in Table 1.

Table 1. Table of fluorophore excitation and emission wavelengths.

Fluorophore	Excitation Wavelengths (nm)	Emission Wavelengths (nm)
Aminio acids	260–295	280–360
NADH and NAD(P)H	290–295, 340–366	440–470
Flavins	450–488	520–560
Cellulose	250–350	350–500
Chitin	335	413
Lignin	240–320	360
Melanin	469–471	543–548
Sporopollenin	300–550	400–650
Chlorophyll	390–470	630–730
Flavonoids	365	440–610
Carotenoids	400–500	520–560
Alkaloids	360–380	410–600
Nucleic acids (DNA)	270, 320	280–370 and 350–470
Terpenoids	250–395	400–725
Phenolic compounds	300–380	400–500

The predominant fluorescent molecules found in PBAP are the amino acids, which are the fundamental building blocks of peptides and proteins, and are common to all life [27]. Of the 20 candidate amino acids, only tyrosine, phenylalanine, and tryptophan are fluorescent (due to their aromatic components), and have absorption/excitation maxima between 260–280 nm. Of the three, tryptophan is known to be the predominant fluorescent species, with as much as 90% of protein fluorescence being attributable to its presence. This enhanced contribution is due to its higher quantum yield when compared to the other amino acids [24].

It is known that a plethora of structural chemicals, including cellulose, chitin, lignin, and sporopollenin, are common to many microorganisms, and also absorb and re-emit light [24,26,28,29]. Sporopollenin, for instance, is a complex biopolymer consisting of carotenoids and phenylalanine which serves as the outermost shell of atmospheric particles, such as pollen [30]. Several studies have used the fluorescence signature of sporopollenin and other pollen grain components to distinguish them from other particles in laboratory and outdoor settings [31,32]. The exact composition of the observed fluorescence in pollen is likely due to a host of bio-fluorophores, such as phenols (emission between 440–480 nm), carotenoids (emission between 500–560 nm), azulene (emission between 440–460 nm), and anthocyanin (emission between 450–470 and 600–640 nm). While sporopollenin as a structural component exclusively relates to pollen, several other fluorescing structural materials are found in other PBAP species. One such component is cellulose, which is an abundant organic molecule that is found in the cell walls of plants, plant debris, fungi, algae, and even bacteria. It is excited over a broad spectrum (250–350 nm), but exhibits rather weak fluorescence in its pure form. Its fluorescence can however be enhanced by the presence of proximal phenolic compounds, with the resultant maxima being observed between 440–460 nm [24]. Chitin is another structural component that is present in all fungi. It exhibits maximum fluorescent emission at ~410 nm and its excitation maximum is observed at ~335 nm [24,33]. Other structural chemicals, such as lignin, one of the most plentiful polymers that is found in the natural world, has also been noted as a fluorescent component observed in certain PBAP, particularly in the cell wall of plants and algae [24]. Lignin exhibits fluorescence emission maxima at ~360 nm upon excitation at wavelengths ranging from 240 to 320 nm [34].

Coenzymes are further category of fluorescent PBAP components that contribute to atmospherically relevant bioaerosol fluorescence. Coenzymes, such as Nicotinamide Adenine Dinucleotide (NADH) and Nicotinamide Adenine Dinucleotide(P)hosphate (NAD(P)H), are typically present in many PBAP. These coenzymes can be utilized as markers for cell life due to their rapid depletion within several hours of cell death. These coenzymes are directly excited at 340 nm, but can also be excited at 295 nm when energy transfer from nearby photo-excited species occurs [24].

Vitamins and flavins are also capable of contributing to observed fluorescent signals from PBAP. Flavins act as metabolic redox carriers and are omnipresent in microorganisms. Riboflavin (vitamin B_2) in particular is an important contributor to PBAP fluorescence. Its absorption maximum in solution is at 266.5 nm, with a further broader, lower energy peak being observed at ~450 nm. Its fluorescence maximum is observed at ~525 nm with quantum yields of 0.36 in acetone and 0.37 in dioxane [24,35]. Other vitamins, such as vitamin A, C, D, K, and the other B vitamins are also potential fluorescent contributors, and have been previously discussed in detail [24].

Given the wide variety of colors exhibited by PBAP, it should come as little surprise that PBAP can contain many differing pigments. Many of these pigments are fluorescent, and, therefore, likely contribute to overall PBAP fluorescence emission. Pigments, such as chlorophyll-a, chlorophyll–b, and melanin, are ubiquitous in nature and are present in various environmentally significant aerobiological organisms. Both fungal spores and bacteria have been found to have high melanin content. The presence of chlorophyll-a has been suggested as a potentially useful individual marker for the discrimination of grass pollen and other atmospherically relevant PBAP [36]. The Chlorophylls are generally excited between 390–470 nm, yielding a distinctive emission between 630–730 nm. Melanin, in contrast, has absorption maxima between 469–471 nm, with a prominent emission band between 543–548 nm.

Nucleic acids (DNA) are another biofluorophore with the potential to add to observed PBAP fluorescence signals. Solution-phase DNA fluoresces between ~280–370 nm upon excitation at 270 nm, with the emission maxima shifting to between 350–470 nm when the excitation source is changed to 320 nm [37]. Those ranges are the same as those that are expected for pollen and fungal spore fluorescence [31,36], however it should be noted that the fluorescence intensity of DNA is rather weak due to its low quantum yields of 10^{-4} to 10^{-5}, and, as such, is not a significant contributor to overall FAP signal intensity [38,39].

Secondary metabolites, such as alkaloids, terpenes, and phenols represent other classes of fluorescent molecules present in a variety of PBAP. The terpenoid's fluorescence wavelengths range between 420 and 480 nm [26]. This spectral range originates from changes in the extent of conjugation that is found in the larger terpenes, with shifts to longer wavelengths associated with increasing conjugation. It has also been reported that several monoterpenes exhibit emission between ~405–430 nm when excited between 310 and 380 nm [24]. Of the terpenoids, azulenes have been extensively studied, as they are known constituents of pollen grains. Azulenes, when linked with cellulose, exhibit fluorescence with two emission peaks apparent, the first between 440–460 nm and the second between 620 and 650 nm. Phenols are another secondary metabolite that can be observed on the surface of biofluorophores such as sporopollenin, or imbedded in the surface of cell walls. Many phenolics are well known fluorophores in their own regard with emission observed between 400–500 nm when excited in the UV range [40]. Finally, one of the most varied of the secondary metabolites are the alkaloids, which occur in microorganisms, such as fungi and bacteria, amongst others. Alkaloids are a diverse group of natural plant compounds, which contain at least one nitrogen in a heterocyclic ring [26,41]. Given the wide variety of alkaloids that are found in nature, it is not surprising that this class of compound exhibits wide variations in the observed excitation and emission spectral ranges. Earlier studies have noted excitation ranges between 360–380 nm, leading to fluorescence in the visible spectrum between 410–600 nm [24,26,41].

1.2. Interferents—Non-Biological Compounds

Fluorescent compounds are ubiquitous in both biological and non-biological airborne particulate matter. This presents significant challenges when measuring fluorescence on atmospheric samples due to the contribution of non-biological derived fluorescence to the overall fluorescence intensity, which can lead to a potential overestimation of FBAP concentrations [24]. Pöhlker et al. previously reviewed several classes of possible interferents which is summarised below.

HULIS is a heterogeneous mixture of compounds that are resulting from the natural decay of biological material. It is ubiquitous in nature and constitutes a significant portion of the organic aerosol fraction [24]. Due to the inhomogeneity of humic matter, the composition of the material varies leading to variability of the nature and quantity of fluorophores present. The fluorescence of the soluble HULIS fraction, has been previously categorised using excitation-emission matrix (EEM) plots, according to two modes, namely humic–like and protein-like fluorescence. The humic-like fluorescence has been observed at three spectral regions ($\lambda_{ex}/\lambda_{em}$): (i) humic-like (UV excitation), 237–260 nm/380–460 nm; (ii) humic-like (visible excitation) 300–370 nm/400–500 nm; and, (iii) marine humic-like 312/380–420 nm [24]. The protein-like fluorescence modes have been denoted as tyrosine-like at 375 nm/340 nm and tryptophan-like at 275 nm/340 nm [42–44].

SOA forms as a result of atmospheric multigenerational oxidation of both man-made and natural volatile organic compounds. These multistep oxidations have the potential to yield large varieties of new compounds with functional groups differing from those with respect to the parent VOC. For example, the autofluorescence of laboratory produced limonene and γ-terpinene SOA was examined by Bones et al. [45], who found strongly enhanced fluorescent emission of the SOA when aged in conjunction with ammonium compounds or amino acids [45]. They noted four fluorescence modes ($\lambda_{ex}/\lambda_{em}$) at: 280 nm/420 nm, 300 nm/360 nm, 340 nm/440 nm, and 425 nm/490 nm. Mineral dust occurring in both fine and coarse modes represents a major component of the global atmospheric aerosol [46–48]. These mineral dusts can contain a host of luminescent compounds, including transition metal and rare-earth cations, amongst others. Bozlee et al. [49] used LIF to examine a range of natural minerals including silicate, carbonate, phosphate and sulfate minerals, and found that they exhibited emission bands at ~500 nm and ~700 nm when excited at 266 nm and 355 nm [49]. Given the observed emission characteristics for a variety of minerals, it is reasonable to assume that mineral and rock dust may act as interfering FAP under certain circumstances. PAHs are a class of compounds that are formed by the incomplete combustion of organic matter. They are ubiquitous in nature and are derived from both man-made and natural sources. These compounds may be present as semi-volatile species in gas or particulate phases, or absorbed on organic aerosol particles [50,51]. Many PAHs are highly fluorescent, and emit over wide spectral regions, ranging from 300–460 nm and 310–540 nm. They are also often present as mixtures of differing PAHs, which can lead to complex EEMs [52]. Of particular interest to this review is the impact of soot on FBAP measurements. It is known that PAH can concentrate on the surface of soot particles that are derived from gasoline and biomass burning. Fluorescence studies of soot particles has noted that emissions emanating from these soot constituents can often be weak due to fluorescence quenching by the bulk material [53,54]. However, recent work carried out by Savage et al. [55], which sought to characterize WIBS fluorescence thresholds, concluded that soot particles can yield sufficient fluorescence to interfere with WIBS FBAP measurement depending on the soot's provenance [55]. In particular, they noted a diesel soot exhibited high median fluorescent intensity, and suggested that increasing the baseline threshold slightly would not significantly reduce the fraction of these molecules that are considered fluorescent. They further suggest that these could reasonably present as false positive counts when subjected to most characterisation schemes.

2. Instrumentation and Operation

This section outlines the operational parameters and the associated literature for the most currently utilized commercially available instruments.

2.1. UV-APS: Ultraviolet Aerodynamic Particle Sizer

The Ultraviolet Aerodynamic Particle Sizer (UV-APS) was the first commercially available single particle fluorescence-based, real-time biological aerosol sensors. The commercial models are based on a prototype instrument that has been detailed previously [56]. To determine the fluorescence/sizing signals pertaining to a wide variety of different PBAP species, the UV-APS has been a central feature of extensive indoor and outdoor field campaigns, as well as laboratory-based experiments [23,57,58]. The instrument evaluates the aerodynamic size and total fluorescence intensity of individual particles, in addition to their concentrations. A laser is used to determine the particle size, as well as to induce PBAP fluorescence.

The UV-APS determines the sizes of particles in a different manner to the other devices discussed below. The UV-APS determines the particle aerodynamic size (D_a), as opposed to optical instruments that estimate optical size based on optical scatter (Mie theory). The D_a is determined by measuring particle velocity relative to air velocity within an accelerating airflow. The time of flight of each particle is measured as the particles in the flow pass through two sequentially positioned laser beams (680 nm). The particle size is then obtained by collecting the scattered 680 nm light, using a suitable detector, followed by comparison to a calibrated library of size values [59,60].

The instrument samples ambient air with an overall flow rate of 5 L min^{-1}. This flow then bifurcates and 1 L min^{-1} of the flow is used as the sample flow. The remaining air is channeled in a laminar sheath that directs and focuses the particle stream to the center flow. Preceding the size parameter measurement, the particle fluorescent counts and intensities are measured using a 355 nm diode-pumped, frequency-tripled Neodymium:Yttrium Aluminium Garnet (Nd:YAG) laser. An ellipsoidal mirror is then used to capture any fluorescent emission from excited particles, with both long pass (410 nm) and short pass filters (630 nm) being used to differentiate between emission and scattered light. The sensitivity of photomultipler tubes (PMT) decreases dramatically above 600 nm, meaning that only fluorescence signals between 410 and 600 nm are actually measured. The number of particles, as well as their aerodynamic size and fluorescence intensities, are then recorded. The UV-APS has seen significantly used in a wide variety of locations and environments, the majority of which are described below.

2.1.1. Laboratory-Based Studies

UV-APS laboratory experiments have mainly focused on evaluating its performance, examining differing particle types, or exploring it as a method to assess other devices [61–82]. In an attempt to understand the response and variance of UV-APS signals, initial laboratory studies were directed towards the aerosolisation of known biological particles in parallel to the aerosolisation of their pure fluorophore components, such as NAD(P)H coenzymes and riboflavin. Agranovski et al., 2003 nebulized aqueous solutions of NAD(P)H and riboflavin of different concentrations into the UV-APS to ascertain whether the sensitivity of the instrument was sufficient to detect these compounds at concentrations that are characteristic of bacterial cells in batch cultures [62]. The results suggested that the amount of NAD(P)H present within injured cells was below the necessary concentrations that are required for detection by the UV-APS (i.e., below the required sensitivity threshold), thus suggesting a possible limitation in the ability of the UV-APS to detect total biological particles. A substantial amount of work has also been performed using the UV-APS to directly detect bacteria, as well as examining the influence of the physiological age and bacterial stress on their ambient fluorescence signals [67,83]. In these studies, Agranovski et al. [83] implied that the size of particles could play a role in the apparent absence of signals for certain bacterial spores, a notable example of which is *B. subtilis* [67]. These earlier studies of the UV-APS, deemed the fluorescence signal observed as a proxy for viable biological particles [67,83]. This may, or may not have been the case given the myriad of fluorophores present in PBAP and the array of chemical particles that fluoresce in the same ranges. Other studies aimed to evaluate the selectivity, sensitivity, counting efficiency, and the detection limits of the UV-APS for several biological (*Bacillus subtilis* spores or vegetative

cells and *Pseudomonas fluorescens*) and non-biological (NaCl, latex, peptone water, and nutrient agar/broth) particles [83]. The counting efficiency of the fluorescent particles was shown to depend on the particle concentration, with the upper limit of detection of the UV-APS being assessed at ~6×10^4 particles/L [83]. Other work has focused on the capabilities of the technique for evaluating the properties of *Penicillium* and *Aspergillus niger* in comparison to results obtained using an AGI-30 impinger [82]. Good correlations were obtained between both instruments (r = ~0.9) for each of the fungal species, and the lower detection limit was determined to be 100 particles/L^{-1} [82]. The effects of aging on the fluorescence and physical properties of the fungal species were also examined. For example, it was noted that an increasing age led to increases in particle sizes, but was also associated with a decrease in the number of spores that were fluorescent [61]. Importantly, the findings pointed to the ability of the UV-APS to differentiate between two types of fungal spores, albeit only in a laboratory setting and under strictly controlled conditions. Based on this study it was concluded that similar experiments would not be feasible in an outdoor (field) environment [61].

As described above, the first wave of laboratory studies focused on the evaluation of the instrumental performance of the UV-APS. This phase was followed by a variety of other investigations, which began to apply the UV-APS technique in more diverse studies, including the assessment of cleaning appliances, such as vacuum cleaners, as potential vectors for bacterial distribution. In the evaluation of the cleaning appliances, twenty-one vacuum cleaners were assessed for a host of parameters, such as the emission of ultra-fine, fine, and course particulate matter, as well as concentrations of bacteria. Significant variability in the release of all particles types was observed across the 21 cleaners. For the emission of particles sizes ranging from 0.54 to 20 µm the concentrations reached 4.0×10^4 to 1.2×10^9 particles/min. It was concluded that vacuum cleaner emissions contributed substantially to the indoor exposure of both total aerosol particles and bacteria [63].

The UV-APS has also been employed to evaluate different types of indoor and outdoor bioaerosol instrumentation. For example, the widely used SKC BioSampler was compared to the UV-APS to examine its collection efficiencies, and the size resolution parameters of biologically viable aerosols [63,70].

The instrument has also been used to ascertain the effect that simulated atmospheric conditions have on biological particle fluorescence. This behavior was assessed by developing a custom laboratory system that used a rotating drum to expose bio-particles to varying concentrations of ozone [73]. While other fluorescent instruments that were used during this work noted a modest blue shift in the emission of biological particles and decreases in fluorescent intensity, no significant changes were seen in the integrated fluorescence (430 nm to 580 nm), as measured by the UV-APS. Roschina et al. studied the changes in the autofluorescence spectra of intact pollen upon exposure to ozone [84]. They determined that the fluorescence maximum at 530–550 nm disappeared in carotenoid-containing pollen, and a new maximum, occurring at 475–480 nm, appeared. The authors suggested that this new peak was associated with the formation of lipofuscin-like substances due to a correlation with the position of the newly observed peak and extracts taken from the samples [84].

2.1.2. Field-Based Campaigns

A number of field campaigns have been undertaken utilizing the UV-APS system, which are summarized in Table 2. Based on this summary, it is clear that the UV-APS has been utilized in a multitude of differing field environments, ranging from rainforests to densely populated urban environments as well as industrial settings such as waste water plants. For instance, the concentrations of fluorescent particles in the semi-urban location of Mainz, Germany were measured during a four-month campaign. Pronounced diel cycles (i.e., 24-h cycles) were noted for fluorescent particles during all of the months, with maximum concentrations sampled during early/mid-morning. These trends and diel cycles were also noted in several other studies [22,57]. The arithmetic mean over the measurement period (four months) for the concentration of coarse fluorescent aerosol particles (FAP) was ~3×10^{-1} L^{-1}, which equated to ~4% of the total coarse particle number (>1 µm). This indicates that while the overall fraction of FAP may be low, its contribution to the

total particles load is measurable and non-negligible. Correlations of weather variables with total particle concentrations and FAP were also undertaken in this work, and showed a quantitative increase in fluorescent number with relative humidity (with variable time offset and low correlation coefficient). Wind direction, on the other hand, yielded no correlation of statistical significance. Similarly, a UV-APS was located during the wet season in the rainforests of central Amazonia, during a campaign entitled AMAZE-08 [57]. The five-week campaign from February to March 2008 showed that FAP particles sized >1 μm exhibited median and quartile concentrations of $7.3 \times 10\ L^{-1}$ and $4.0–13 \times 10\ L^{-1}$, respectively. Diel cycles, with early morning peak fluorescent particle counts, were again noted throughout the course of the sampling period. As observed in previous studies, the fluorescent particle count and the percentage fluorescence of the total particle count correlated well with the ambient temperature and humidity. The study also observed that lower temperatures and high relative humidity were linked to increases in both of the parameters. When comparing the Mainz campaign with that of AMAZE-08, it is interesting to note that the average concentrations were twice as great for fluorescent particles in the Amazon versus the urban site in Mainz. The study also revealed that the fluorescent particles that were sampled during the AMAZE-08 campaign made up on average ~24% of the total particle concentrations (>1 μm) and ranged between 11% and 41% (quartile range) [57].

While these two studies were not comprehensively contrasted in the literature, other researchers have directly compared the measured particle concentrations and trends at sites with significant geographical separation. One study reported seasonal cycles and trends of fluorescent aerosol particles (FAP) from a forest in Hyytiälä, Finland as compared to a semi-arid forest in Colorado, United States of America (USA) [85]. The work was conducted over ~18 months at the Finnish site, while 10 months of sampling was undertaken in Colorado. This study represents one of the longest continuous sampling campaigns undertaken utilizing real-time fluorescence instrumentation [85]. The FAP that was measured in both locations were significantly higher in summer than those observed in winter, with the concentrations recorded as a factor of 12× and 5× greater between the seasons in Finland and Colorado, respectively. The authors suggest that low temperatures and reduced sunlight during winter hindered the release of PBAP. Indeed, the more extensive snow cover reported at the Finnish site was deemed to be a major contributor to its lower winter FAP concentrations. Average size distributions at each site exhibited peaks between 1.5–6 μm. The Finnish site consistently showed a dominant narrow FAP peak at ~3 μm, in addition to discreet modes at ~1.5 and ~5 μm, whereas the Colorado site showed broader peaks at 1.5 and 5 μm. This suggested that different biological species with different size modes were present at the two sites. The work also reported trends between FAP concentrations and meteorological parameters such as relative humidity (RH). In both settings it was shown that FAP correlated well with daily patterns of RH for the duration of both the summer and winter seasons. Summer months at each site exhibited mean FAP numbers that increased with RH, but at the Finnish site, RH values above ~82% led to a significant decrease in FAP concentration. It was speculated that the source of this decrease was dew formation, which may have inhibited bioparticle release. The RH was not the only meteorological parameters that correlated with bioparticle concentrations. Rain during the summer at each location led to pronounced increases in both fluorescent and total particle concentrations of FAP peak particle sizes at ~2 μm. It was also noted that the particle concentration increased with rain intensity [85].

The UV-APS has not only been located in semi-urban, tropical, or rural settings, but also at locations with potentially significant levels of anthropogenically produced bioaerosols. A recent study analyzed data obtained from a UV-APS placed in seven different sampling sites at a waste treatment facility [86]. The size distributions of the fluorescent particles were determined at each of the locations to assess whether varying trends between locations could be observed. The authors noted that particles less than 2 μm were present in the highest concentrations at the biological reaction basin (1.300–3.867 particles/L) and within the on-site office building (1.133–3.667 particles/L). With respect to the larger fluorescent particles, the sludge-thickening basin was found to contain the highest concentration of particles >2 μm, and exhibited levels of up to 6.533 particles/L. The work suggests

that there were major measurable differences between the seven sampling sites, although the size distributions at the locations were similar. It was also noted that the size range between 3–4 µm included the highest concentration of fluorescent particles at the majority of the test locations, suggesting that fungal species and/or bacterial aggregates were contributing to the loading. The one location, which yielded differing results regarding the dominance of the 3–4 µm size range, was the office building, with a main fluorescent peak being observed ~1.5 µm. The most likely explanation for the fluorescence signals is that humans are acting as the release vector for the bacteria [86].

The final field study under review was a campaign in which a UV-APS was operated continuously at a tropical high-altitude site over 11 weeks during the monsoon and winter seasons. Mean fluorescent particle numbers of 20 L^{-1} were recorded during the campaign for the monsoon season [87]. Interestingly, this number accounted for only ~2% of the total particle load that was found at the site, which was much lower than the fractions noted at the many of the other field locations mentioned above. Again, the predominant peak size mode that was seen during the campaign was ~3 µm, which was attributed to fungal spores. This assertion was supported by reference to scanning electron microscope (SEM) images of the samples. Mean fluorescent particle concentrations were seen to vary over the months that encompassed this campaign with values 30, 7 and 15 L^{-1} sampled for June, July, and August, respectively. The total particle count was far higher than the potential bio-particle number (i.e., FAP concentration) that was measured throughout the campaign. The measured concentrations were heavily linked with meteorological parameters, such as wind direction and precipitation. For instance, periods with persistent intense rainfall and westerly/southwesterly winds were associated with negligible total (1300 particles L^{-1}) and negligible fluorescent particle concentrations (5 particles L^{-1}), and no diurnal trends were documented during these periods. Conversely, fragmented rainfall coupled with a northerly wind saw a tenfold increase in fluorescent particles with diurnal variations evident. Finally, campaign-averaged fluorescent number concentrations showed reasonable correlation with daily patterns of meteorological parameters: relative humidity had an $R^2 = 0.58$ (positive correlation); temperature showed a negative correlation ($R^2 = 0.60$) and finally wind speed exhibited a negative correlation ($R^2 = 0.60$) [87].

Table 2. Published studies of ambient Fluorescent Biological Aerosol Particles (PBAP) detected by Ultraviolet Aerodynamic Particle Sizer (UV-APS).

Location	Site	Length	Particle Type Analyzed	Concentration Values (Mean or Peak)	Reference
Mainz, Germany	Semi-urban	4 months	FAPs (1–20 µm)	30 L^{-1} (mean)	[23]
Central Amazonia, Brazil	Rainforest	~1 month	FAPs (>1 µm)	73 L^{-1} (mean)	[57,88]
Colorado, USA	High altitude	~2 months	FAPs (>0.54 µm)	30 ± 10 L^{-1} (mean)	[89]
Colorado, USA	Semi-arid forest	10 months	FBAPs	15 ± 24 L^{-1} (spring) (mean); 30 ± 30 L^{-1} (summer) (mean); 17 ± 31 L^{-1} (fall) (mean); 5.3 ± 6.3 L^{-1} (winter) (mean)	[85]
Colorado, USA	Semi-arid, forest	35 days	FAPs (0.3–20 µm)	30 L^{-1} (dry periods) (mean)	[90]
Colorado, USA	Forest	~1 month	FAPs (0.5–20 µm)	~400 L^{-1} (peak)	[91]
Beijing, China	Waste water plant	NA	FAPs	>2 µm 6.533 L^{-1} (peak); <2 µm 3.867 L^{-1} (peak)	[86]
Beijing, China	Urban	2 weeks	FAPs	500 L^{-1} (peak)	[92]
Beijing, China	Subway	~1 month	FAPs	2.5 × 10^3 L^{-1}	[93]
Multiple sites, China	Urban	March–April	FAPs (0.5–20 µm)	N/A	[94]
Multiple sites, China	Urban	12 days	FAPs	5 to 470 L^{-1} (range), 79 L^{-1} (mean)	[95]
Helsinki, Finland	Urban	23 days (winter); ~60 days (summer)	FAPs (0.5–15 µm)	10–28 L^{-1} (range), 15 L^{-1} (mean)	[96]

Table 2. *Cont.*

Location	Site	Length	Particle Type Analyzed	Concentration Values (Mean or Peak)	Reference
Hyytiälä, Finland	Boreal forest	18 months	FAPs	15 ± 24 L^{-1} (spring) (mean); 46 ± 48 L^{-1} (summer) (mean); 27 ± 32 L^{-1} (fall) (mean); 4 ± 46 L^{-1} (winter) (mean)	[85]
Hyytiälä, Finland	Boreal forest	2 years	FAPs (1–20 μm)	500 L^{-1} (peak)	[97]
Killarney, Ireland	Rural	~1 month	FAPs (0.5–20 μm)	~55 L^{-1} (peak)	[98]
India	High-altitude site	11 weeks	FAPs (>1 μm)	20 ± 20 L^{-1} (mean); ~520 L^{-1} (peak)	[87]

2.1.3. Agricultural Campaigns

There are numerous situations where human activity directly contributes to the release of BPAP. Farming activities, both in the cultivation of crops and in the husbandry of livestock, have been known to harbor sources of PBAP, as well as emitting great quantities of them due to the various processing methods that were utilized [99,100].

The UV-APS has been deployed in agricultural locations in an attempt to assess the total particle count and biological fraction of the airborne particulate matter that is produced by farming activities. Aerosol loads inside a swine containment building were monitored as a function of normal activities, such as the flushing of effluent with recycled water [101]. These measurements were performed in conjunction with a six-stage Andersen microbial impactor and AGI-30 impingers. The UV-APS concentration measurements were observed to be very high, with FAP numbers being noted at levels 12× higher than those that were measured in a non-agricultural outdoor environment taken by the group. Indeed, total particles were seen to be 5× higher than those that were generally present outdoors. Both of the measurements (total and fluorescent count) were recorded to be ~10^3–10^4 particles per L for the campaign. Of significant interest with regard to health-related aerosols, was the finding that ~50% of the sampled particles were in the fine fraction of particulate matter (<2.5 μm).

When compared with the other instrumentation that were used in the campaign, the UV-APS fluorescent counts were an order of magnitude higher than the concentrations of microorganisms that were measured using the AGI-30 impingers. This discrepancy is expected since the AGI-30 measurements represent culturable microorganisms rather than fluorescent counts, and thus would be expected to present differing total values. However, the overall trends in the concentration changes that were measured using fluorescent counts followed those of the culturable airborne microorganisms, with an R^2 value of 0.53 being returned [101].

2.1.4. Indoor Campaigns

The UV-APS has been deployed in a number of indoor sites, such as hospitals, examination rooms, lecture theatres, and flood-affected housing [102–106]. Such studies have generally examined the release of particles and the calculation of emission factors.

One such study focused on the reporting of fluorescent particle counts in two hospitals in Brisbane, Australia. Of interest was the differing patient composition within both of the facilities, with one of them being an adult hospital, and the other a pediatric facility. The UV-APS was used to identify fluorescent particle sources, as well as their contribution to total particle concentrations. A significant difference was seen between the two hospitals for both fluorescent and non-fluorescent particles, with both being observed to be higher in the adults' hospital when compared to the children's hospital ($p < 0.01$). Indeed, FAP in the adults' hospital were noted to be double that of the children's infirmary, with particle number values of 60 and 30 particles/L beng measured in the respective hospitals. Non-fluorescent particles were a factor of 4 greater in the adults' hospital when compared to the children's one (1.20×10^3 particles/L vs. 0.33×10^3 particles/L,). It was noted that while the overall

fluorescent concentrations were higher in the adults' hospital, the proportion of fluorescent particles was higher in the children's hospital [105].

Another investigation used the UV-APS to determine the effects of hospital bronchoscopy examinations on the aerosol composition in bronchoscopy rooms [103]. The research sought to determine the number-concentrations of both fluorescent and non-fluorescent particles, in addition to determining the size distribution of each cohort. The concentrations of the non-fluorescent and fluorescent particles (which were assumed to be biological in nature) were significantly higher ($p \leq 0.05$) during the bronchoscopy examinations, when compared to previously measured reference values (i.e., bronchoscope insertion tasks appear to yield significantly higher concentrations of fluorescent particles). The average particle sizes of each of the fluorescent and non-fluorescent particle samples were shown to be 2.9 µm and 0.9 µm, respectively, indicating that the fluorescent fraction was indeed biological in origin. Finally, the particle number for each decayed at different rates, with the fluorescent particles returning to reference concentration ranges within 15 min of the cessation of activity and the non-fluorescent particles requiring to 95 min to return to reference ranges. This is not an unreasonable finding given the average sizes for each of the particle classes that were recorded, as smaller particles tend to remain suspended for longer periods when compared to larger ones [103].

The bioaerosol emissions emanating from humans have also been investigated with the use of a UV-APS. The study involved a sample of twelve healthy adults who were monitored in a controlled environment. The work examined the effect that two different respirators ("Doctors masks" and N95 masks) had on such emissions. Substantial increases in the number of FAP were recorded within the controlled environment when five people were present. Within this environment, the bioaerosol concentration increased by 107% (vs. reference measurement) within 30 min. Based on this data, an average emission rate of 8.4×10^5 fluorescent particles/person/hour was calculated. Lower concentrations increases were associated with the use of respirators, with ambient bioaerosol concentration increasing by 81% (vs. reference) when N95 masks were used, and 31% (vs. reference) when Doctors masks were worn. It was concluded that bioaerosol emissions from exhaled breath accounted for about 17% of the observed increases in the controlled environments. Bioaerosol concentrations within school classrooms were also measured during this study, and a 50% increase was noted with human occupancy [102].

Other research has been performed regarding the effect that human occupancy has on FAP counts in common-use indoor environments. The total number of particles and FAP concentrations in a classroom ranging in size from 1 µm to 15 µm were recorded for a number of occupied (n = 18) and unoccupied (n = 8) days over a period of one year [104]. As expected, higher emission rates were documented for the occupied days with a mean emission value of 2×10^6 fluorescent particles/person/hour noted. This value was related back to metabolic CO_2 production, with each gram of metabolic CO_2 being calculated as equivalent to 9×10^4 particles. Day-to-day and seasonal variations in the data were small, therefore, the variability suggested that a number of factors, including levels of occupancy, occupant activities, and the operational state of the ventilation system each contributed to the observed results. In particular, the ingress and egress of the occupants were related to high releases of fluorescent particles with estimated mean emissions of 0.8×10^6 particles per transition per person. These fluorescent particle releases are likely due to the turbulence that is caused by such transitions. The UV-APS also analyzed the size regimes of these particles and noted a mode between 3–4 µm. These results are very similar to those that are observed for work performed in outdoor environments [104]. Overall, the reviewed indoor studies reveal that a host of everyday work related activities can significantly increase total and fluorescent particle concentrations. These activities can range from the active production of FAP, as observed with agricultural activities and certain hospital procedures, to more passive sources, including the effect of transitioning people between locations, along with the emissions of physiologically aerosolized biological particles that are generated by humans.

It appears from the reviewed literature that relatively few UV-APS bioaerosol studies of indoor environments have been undertaken. While interesting results have been presented, the general dearth of long-term and large scales studies does not allow for a more comprehensive understanding of the sources and fluctuation characteristics of biological particles that are linked to human occupation. Further research in this area could yield significant insights, which would allow for a better description of the provenance and indoor transport characteristics of these bioparticles.

2.1.5. Ice Nucleation Studies

The potential link between bioaerosols and ice nucleation (IN) has become an area of increased research focus. Studies, such as BEACHON-RoMBAS in Colorado, USA, utilized a range of instruments, including a UV-APS, to study the apparent relationship between increased IN numbers and rainfall [107]. The work suggested that concentrations of ice nucleating particles are bolstered subsequent to precipitation events, with measurements indicating that the increase was about an order of magnitude. Of particular note, was that IN activity from −15 °C to −25 °C was greatly enhanced [107]. This finding is of considerable interest given that biological INPs are implicated in the process of inducing nucleation at higher temperatures than other atmospheric (chemical) species [15]. Although the correlation between IN and fluorescent particles was notable, it was suggested that the explicit mechanism of IN remains as yet unidentified. The fluorescent particles linked to the rain events responded in an approximately linear fashion (correlation coefficient, R^2 = 0.94) to those of the IN, suggesting that the fluorescent particles are indeed serving as IN during the rain events. Fluorescent counts were seen to far exceed IN during such rain episodes, with concentration values exceeding those of the IN by about a factor of four during the rain event [107]. The correlation of FAP numbers with ice nucleation particles led to the conclusion that a significant fraction of the precipitation generated ice nuclei were biological in nature. This result is in agreement with previous reports in the literature [88,107].

The campaign above also featured additional work utilizing a number complementary sampling devices in conjunction with a UV-APS [25]. The results of this study led to the conclusion that the greatest increase in bio-particle numbers and IN occurred in the size range between 2–6 μm, which is characteristic of bacterial aggregates and fungal spores. DNA analysis pointed to the discovery that two species, *Isaria farinose* and *Acremonium implicatum*, were implicated in the observed IN activity. These fungal spores had not been previously associated with any ice nucleation phenomena. This work demonstrated that the UV-APS, when used in tandem with other sampling devices and techniques, can give useful results on FAP identity as well as number-concentrations [25]. However, it should be noted that given the limited number of studies in this area, along with the methodologies that were employed, further research is still required to fully elucidate the interplay between bioaerosols and IN.

2.2. WIBS: The Wideband Integrated Bioaerosol Sensor

The Wideband Integrated Bioaerosol Sensor (WIBS) is a single aerosol particle fluorescence monitor that uses light-induced fluorescence (LIF) to detect fluorescent aerosol particles (FAP) in real-time. The original instrument was invented by Professor Paul Kaye and co-workers at the University of Hertfordshire. It is now commercially available from Droplet Measurement Technologies (DMT), and is one of the most widely-used instruments for monitoring PBAP in real-time. The WIBS was originally developed for defense applications to enable the detection of airborne particles [108]. It offers the ability to characterize the size and asymmetry (shape) of individual fluorescent and non-fluorescent particles by assessing the forward and sideways optical scatter, along with the spectrally unresolved fluorescent intensity of each particle at a millisecond time resolution. There have been several versions of the WIBS available, from Models 3 and 4 prototypes, to the commercial version 4A.

With regard to their operation, there are a number of differences between the prototype WIBS-4 and commercially available WIBS-4A. The prototype WIBS-4 draws in ambient air at a rate of

2.4 L min^{-1}. Approximately 2.2 L min^{-1} of the initial aerosol flow is filtered and reintroduced as a sheath flow to confine the remaining 0.2 L min^{-1} sample [108]. With the commercially available WIBS-4A instruments, the analyte particles are pumped into the main optical chamber at a rate of 2.5 L min^{-1}. Part of this flow, ~0.3 L min^{-1}, is then directed as sample flow. The remaining 2.2 L min^{-1} of the air flow is filtered before forming a sheath flow to constrain the sample flow as a vertical column, which sequentially aligns the incoming particles [109]. Both WIBS models use a combination of the sheath flow and a small bleed flow to constantly purge the optical chamber of any extraneous particles. The initial detection of the particle uses a continuous-wave red diode laser at 635 nm that illuminates the particles flowing into the optical chamber. Scattering of the laser light is used for both the sizing of particles (based on Mie theory) and to determine a basic particle "shape" using a so-called asymmetry factor (AF). As with most optical particle counters, the WIBS-4 and WIBS-4A apply a particle size calibration that is based on a theoretical curve, which assumes that the particles are spherical and of a specified refractive index. Both prototype and commercial WIBS use a calibration curve that is calculated using standard monodispersed polystyrene latex (PSL) microsphere aerosols. These spheres have a quoted refractive index of 1.58 $\pm$ 0.2 [109]. As the calibration curve is based on PSL spheres, the size data that is produced should be treated as an estimate, especially when measuring spherical particles of disparate refractive index or non-spherical solid particles. The WIBS-4 prototype contains a size selection utility allowing for the user to select one size fraction of the ambient air sample to perform data analysis on. In practice, this is controlled via a sensitive dual gain function with two switchable settings: High Gain (HG) and Low Gain (LG). Smaller size particles that are in the range between 0.5 and 12 μm are monitored in HG, whereas larger sized (more highly fluorescent) particles in the range between 3 and 31 μm are detected in LG. The commercially available models (WIBS-4A) have a single gain setting, which evaluates particles between 0.5–20 μm. Use of the gain settings affect WIBS particle sizing range, however, it should be noted that this is an instrumental limit rather than a fundamental limit with regard to light scatter sizing. Particle shape is assessed through the azimuthal distribution of the forward scattered light. The forward scattered light falls on a quadrant PMT detector where the scattering pattern of the particle is sampled at four angular offsets. For each of the scatter intensities that are recorded by the quadrants, the root-mean-square variation around the mean value outputs produces a numerical value between 0–100 AF units, with 0 being a perfect sphere and 100 denoting long rod-like fibrous particles. The fluorescence characteristics of the individual particles are then interrogated using two xenon flash lamps (Xe_1, Xe_2). They are tuned to excite at the maxima absorption wavelengths of the biofluorophores tryptophan (280 nm) and NAD(P)H (370 nm), by delivering two sequential ultraviolet pulses at 280 nm and 370 nm. Fluorescence emission following these excitation pulses is detected in two detector bands: 310–400 nm (Band I) and 420–650 nm (Band II). Thus, once a particle has been detected by the laser (after ~10 μs), the first xenon light source (280 nm) is triggered which induces fluorescence that is detected in two bands. Following this sequence, the second xenon flash lamp (370 nm) is triggered (after a further 10 μs) resulting in another excitation of the particle. Subsequent measurement in both the first and second detector bands follows, however the wavelength data from the first band (310–400nm) is discarded due to interference from the excitation pulse (370 nm) [110]. Hence, for individual particles, three fluorescence measurements are recorded: (a) Excitation at 280 nm, emission in Band I (termed FL1); (b) Excitation at 280 nm, emission in Band II (termed FL2); and, (c) Excitation at 370 nm, emission in Band II (termed FL3).

While the flash lamps are tuned to excite at the maxima of the biofluorophores tryptophan and NAD(P)H, it should be emphasized that a host of other PBAP fluorophores, such as cellulose and light harvesting pigments, like the chlorophylls, can also contribute to the luminescence signals (*vide supra*). Humic-like Substances (HULIS), Secondary Organic Aerosols (SOA), Polycyclic Aromatic Hydrocarbons (PAH), and other important atmospheric chemicals can also fluoresce in the spectral regions relevant to WIBS technology, but often with much smaller quantum yields than the biologicals. However, the possibility remains that they may still contribute to the overall WIBS data-sets and related FAP numbers. Where results are suspected to have large quantities of these potentially interfering

non-biological materials present, the data analyst must take extra attention when interpreting the WIBS measurements.

There are also several differences in the instrumental configurations of the early prototype WIBS-3 and the WIBS-4. The WIBS-4 included several upgrades from the WIBS-3, such as improvements to its optical configuration, optical filters, UV delivery, and sample inlet system [110–112]. However, the most significant difference was made in the separation of two detection bands. The WIBS-3 has two detection bands that overlap (FL1 = 320–600 nm; FL2/FL3 = 410–600 nm), whereas, within the WIBS-4 and WIBS-4A, this overlap does not occur. This constrains the bands in which a particle fluoresces, allowing for the FL2 channel to more completely differentiate information from the FL1 channel. WIBS data-sets also contain particle numbers, size and "shape" parameters, along with the three individual fluorescence intensity characteristics. Perring et al. [113] conducted a dual campaign using a WIBS-4 in Florida and California and subsequently developed a new annotation system. They categorized particle fluorescence into one of seven types, depending on the three forms of fluorescence signals detected by the WIBS [113]. These categories consider each channel individually (FL1, FL2, and FL3), but also includes all possible combinations, as shown in Table 3. Such cataloguing nomenclature allows for a greater degree of individual particle classification since the particle fluorescence intensities could previously only be placed into one or more of the FL channels, depending on their fluorescence. Thus, the designations used in Table 3 allow for a more detailed understanding of ambient particles fluorescent characteristics.

Table 3. Wideband Integrated Bioaerosol Sensor (WIBS) channel annotation matrix. Channels are matched with excitation wavelength and emission waveband.

Channel	Excitation (nm)	Emission (nm)
A	280	310–400
B	280	420–650
C	370	420–650
AB	280	310–400 420–650
AC	280 370	310–400 420–650
BC	280 370	420–650
ABC	280 370	310–400 420–650 420–650

This categorization system denotes particles that fluoresce above the threshold in only one channel as either types A, B, or C (depending on the excitation and emission wavelengths of the particle, as indicated in Table 3). Particles fluorescing in only two channels are classified as types AB, AC, and BC; while, particles that fluoresce in all of the channels are categorized as type ABC [113]. Using this method of classification, it is hoped that more complex environments can be better characterized by reference to the many different types of FAP which are observed.

The processing of the collected data is arguably the most challenging step in distinguishing between PBAP and interfering non-biological fluorescent compounds. This is in part due to the rather large data sets (>10,000,000 particles with each of the five variables), which can be routinely collected during a campaign. In an effort to simplify the subsequent analyses, the WIBS data is reduced into discrete concentration time-series. In an effort to extract useful data from these large sets, Robinson et al., 2013 have used hierarchical agglomerative cluster analysis [114]. The technique was first applied to the measurement of various fluorescent and non-fluorescent polystyrene latex spheres

(PSL). Excellent separation was achieved, with the cluster analysis successfully classifying the majority of the particles correctly [114]. The methodology was then applied to two separate simultaneous ambient WIBS data sets that were recorded in a forest site in Colorado, USA [114]. The authors suggested the following criteria as essential for WIBS single-particle data analysis: (i) Simplification procedures should not include any assumptions about the types of particles present in the dataset, since this would prevent the identification of PBAP, which have not been previously characterised using similar measurements; and, (ii) As several types of PBAP can be present in a wide range of concentrations, assumptions regarding relative group sizes should not be required. When the analysis method is applied and differences between the WIBS-3 and WIBS-4 are taken into consideration, the average measurement values of the clusters were qualitatively similar. Ambient cluster results were related to aerosol types by comparison of the cluster measurements averages and time-series to the available literature. By applying the cluster analysis to the collected ambient data sets, bacterial agglomerations, fungal smut spores, and other fungal spores were suggested as separate cluster identities. The approach was tested and verified on a controlled data set of PSL measurements, and were successfully applied to a subset of WIBS measurements, with the remaining measurements being accredited to the previously resolved clusters [114].

2.2.1. Laboratory Studies

Many laboratory experiments have been performed to evaluate the counting efficiency of the WIBS. The particle counting efficiency of the WIBS-4 has been measured using polystyrene latex (PSL) microspheres in size ranges between 0.3 and 30 µm [115]. The experiment compared the results of a WIBS-4 particle count to the results that were obtained using a commercially available reference instrument, the condensation particle counter (CPC, TSI, Model 3010, Minnesota, USA) [115]. A parameter termed D_{50} was used to define the diameter of particles with a number concentration ratio for WIBS-4/CPC experiments that is equal to 50% counting efficiency (i.e., WIBS counted 50% of that seen by the CPC). A D_{100} was likewise defined as 100% counting efficiency (i.e., both instruments counted equal amounts at a given size value) [115]. The lower-end counting efficiency curve was then defined in specific size regimes (D_{50} ~0.489 µm and D_{100} ~0.690 µm) [115].

The WIBS-4 sensitivity that was surrounding the analysis and discrimination of biological and non-biological aerosols has also been the subject of many studies (*vide infra*). However, in an effort to distinguish between major classes of airborne microbes and pollen, numerous studies have sought to measure the optical fluorescence signals, which would enable this distinction to be made. The sensitivity for PBAP discrimination using the WIBS-4 was investigated by Healy et al., 2012 [110]. Fifteen samples from two separate taxonomic kingdoms, *Plantae* (8) and *Fungi* (7), along with two non-fluorescing chemical solids (common salt and chalk), were systematically introduced into the WIBS-4, and more than 2000 individual-particle measurements were then recorded for each sample type [110]. The ability of the WIBS-4 to discriminate between chemical particles and the pollen and fungal spores was then explored through the classification of FAP signatures. Discrimination between the particles was made on the basis of five measurable characteristics (size, AF, FL1, FL2, and FL3) [110]. The use of these variables demonstrated that some spore and pollen sample signals could be separated from each other, according to the normalised fluorescence data that was obtained in the FL1/FL3 axis. Most interestingly, grass pollen was shown to be separable from other pollen [110]. Based on these results, it was suggested that using a combination of three-dimensional (3-D) plots of normalised fluorescence coupled with size measurements, may enable the instrument to be used as an early warning system for the presence of bio-aerosols [110].

The sensitivity of a WIBS-4 for discriminating chemical and biological aerosols was evaluated using a series of environmental chamber experiments [116]. The number-concentrations and size distribution of the aerosols in the chamber experiments were measured by an assortment of instruments, including the WIBS-4, an Aerodynamic Particle Sizer, and a CPC. The laboratory tests supported and clarified the accuracy of the previously defined fluorescence thresholds of the WIBS. The results further

demonstrated the ability of the WIBS to discriminate between biological and non-biological aerosols, with the study concluding that some non-biological particles (polycyclic aromatic hydrocarbons, mineral dust, and ammonium sulfate) may cause interference for individual WIBS channel signals. However, it was found that using a combination of two fluorescent channels provided adequate discrimination between biological and non-biological aerosols [116]. For example, the authors found that using a combination of FL1 and FL3 channels, an aerosolised ammonium sulfate-fungal spore mixture could be readily discriminated [116].

Hernadez et al. [117] has compiled an aerobiological reference catalogue of more than 50 pure cultures of common bioaerosols (bacteria, fungi, and pollen) using a WIBS-4A [117]. The catalogue visualizes size, shape, and fluorescent channel emission intensities of the investigated samples, which allows for discrimination between the major classes of airborne microbes and pollen. The main discriminators used were: (i) The utilization of the ABC category nomenclature; (ii) The average fluorescence intensity within each of these categories; and, (iii) The average Equivalent Optical Diameter (EOD) [117]. Based on the application of the discriminators, common fluorescence patterns for each of the bioaerosol classes were observed. For instance, most aerosolized bacterial cultures that accumulated with EOD < 1.5 μm displayed weak fluorescence intensities predominantly in the fluorescence type A category. However, a breakdown of this general trend was noted for *Bacillus subtilis*, which dominated in the AB category. Fungal spores were noted to exhibit a higher EOD range (2–9 μm), but encompassed several fluorescence types: A, AB, BC, and ABC, with most giving rise to type A and AB. Although pollen grain signals overlapped with those of several fungal spores with respect to EOD ranges, the former largely exhibited higher fluorescence intensities because they contain more biofluorophores (due to their larger size). Type C fluorescence was more dominant with fungal spores when compared to pollen grains, which displayed only as BC and ABC types [117]. Unde defined conditions (i.e., relative humidity, temperature and culture conditions), it was suggested that key components of airborne samples could be distinguished by measuring optical diameters and fluorescence intensity [117].

Using the same ABC categorization system as described above, a chamber-type experiment was performed, which used a WIBS-4A to evaluate the release of fluorescent particles that were associated with human shedding while walking [118]. The monitoring was carried out in a small office room (39.5 m^3), with the only air-exchange occurring through air filtration [118]. A mean emission rate of fluorescent particles in the range 1–10 μm was calculated to be 6.8–7.5 million particles/person/hour. This value is equivalent to ~0.3 mg/person/hour. Of the total fluorescent particles, 90% were associated with the categories ABC, AB, and A. Particles in the ABC channel were the highest contributors making up to 40% of the total number (particles > 1 μm) and ~70% of mass emission rates of fluorescent particles [118]. The fluorescent particles demonstrated a lognormal distribution, with a mean geometric diameter within the 2.5–4 μm range. The ABC category showed a higher lognormal size distribution with a value of 4 μm for the mean diameter. This value was 1.5 μm greater than that observed for the A and AB categories. The AF (shape) parameter of the fluorescent particles also increased with size [118]. Another component of this study sought to measure the influence of applied moisturiser (jojoba oil) on the frictional interactions between skin and clothing. The oil application resulted in a significant increase in emissions rates, with factors between 2–5× noted. However, the emissions that were related to the moisturiser were due to smaller particle sizes and the mass emissions rate was lower with moisturiser than without. Moisturiser use also increased the emissions of category A particles, which is a possible indication of abiotic interference that is associated with their use [118].

The instrumental fluorescence detection limit is determined by measuring the fluorescence emission signal when no particles are present in the optical chamber. This is undertaken by putting the WIBS instrument into a setting known as "forced trigger" mode. This mode essentially causes the flash lamps within the WIBS to fire on empty space while the pump is off. Background fluorescent values from the forced trigger mode are then collected for each channel. In general, the average of these values plus 3× standard deviations of the mean fluorescence intensity in each channel (FL1,

FL2, and FL3) are then used as the cut-off thresholds. In more recent times, alternate threshold strategies utilizing increased thresholds to aid in the detection, classification, and discrimination of ambient bio-particles from interfering particles have been suggested [55]. Savage et al. [55] systematically evaluated fluorescence thresholds for the WIBS-4A using sixty-nine types of aerosol material, which included size-resolved biological particles (i.e., bacteria, fungal spores and pollen), and chemical interferents (i.e., soot, smoke and HULIS) [55]. A broad separation between the two classification types was observed using size and shape parameters in conjunction with the Perring (2015) [113] particle classification system. Using these different classification systems, the role that particle size plays in controlling fluorescent properties was assessed. This was carried out with the inclusion of a new threshold calculation whereby the fluorescent threshold was raised from the usual forced trigger (FT) + 3σ to FT + 9σ. This results in weakly fluorescing aerobiologically insignificant particles under the previous threshold being reassigned as non-fluorescent under the new FT + 9σ criteria. The authors concluded that while it does not reduce the fraction of aerosol considered biological, it does significantly reduce fluorescence interference to almost zero for most particle types [55].

Currently, no standard fluorescent calibration method exists for real-time, single-particle fluorescence instruments. However, Robinson et al., 2013 has proposed a method that uses size-selected particles containing a known mass of fluorophore to calibrate the fluorescence detection of a WIBS-4A [119]. This approach was attempted using mixed tryptophan-ammonium sulfate particles to calibrate one detector (FL1) and pure quinine particles to calibrate the other (FL2). Based on the resulting fluorescence and mass relationship data, the tryptophan-ammonium sulfate particles displayed a linear relationship. The pure quinine particles gave non-linear signals, suggesting that only a portion of the quinine mass contributes to the observed fluorescence [119]. Both of the materials produced a repeatable response between observed fluorescence and particle mass. This procedure should provide the data to: establish appropriate detector gains (absolute response); estimate limits of detection; improve the repeatability of instrument set-up; and, enable more meaningful instrument comparisons [119].

2.2.2. Field Campaigns in Ambient Outdoor and Indoor Environments

All versions of the WIBS instrument (3, 4 and 4A) have been used in field campaigns within vastly contrasting settings. All of the studies focussed on the detection and quantification of PBAP concentrations in relation to the total particle load. Many of the studies used standard reference and/or other additional UV-light induced fluorescence (UV-LIF) techniques to assess the capabilities of the WIBS approach [21,98,116,120–122]. Some examples of these campaigns are shown in Table 4. For example, the particle morphology and fluorescence signals (FL1, FL2, and FL3 channels) of aerosolized materials in the size ranges between 0.8–20 μm have been investigated in two dissimilar environments, an urban city center (Manchester, United Kingdom (UK), December 2009) and a remote, tropical forest (Borneo, Malaysia, June/July 2008) [21]. The FL1, FL2, and FL3 channels represented 3%, 6%, and 11% of the total aerosol counts over the Manchester campaign, with two dominant size modes being recorded for the fluorescent material, one at 0.8–1.2 μm and a second at 2–4 μm [21]. A large variation in the fluorescence and total aerosol concentration was evident throughout the day, with non-fluorescent particles peaking between 05:00–10:00 and 17:00–19:00, and the fluorescent particles concentrations peaking strongly at 09:00–10:00. Due to the concentrations of non-fluorescent and fluorescent particles peaking at a similar morning period, it was suggested that the release of SOA particles from traffic activity may have impacted on these results. Given the particle size profile and the fact that SOA can absorb and fluoresce at the same excitation/emission wavelengths that are associated with biological particles, they likely represent possible interferents in this study.

In the Borneo campaign, a clear diurnal pattern was observed under the rainforest canopy, with FAP concentrations being recorded at a minimum of 50–100 L^{-1} in late morning. This period was followed by strong temporal fluctuations before reaching 4000 L^{-1} in mid-afternoon.

Stable concentrations spanning 1000–2500 L^{-1} were measured between midnight and sunrise. Above the canopy, FAP ranged from 50–100 L^{-1} during the day to 200–400 L^{-1} at night. The transient fluctuations that were seen in the under-storey were not observed [21]. FAP accounted for 55% of the total aerosol that was monitored beneath the canopy, and fell to 28% above it (for particles between 0.8–20 µm). Both sites exhibited a size mode at 2 µm < D_o < 4 µm, which consisted primarily of FAP. These accounted for 75% of the under-storey and 57% and above-canopy coarse particles ($D_o \geq$ 2.5 µm) [21]. It was suggested that a potential link between FAP concentrations and relative humidity existed as the highest FAP concentrations were measured at RH $\geq$ 80%. This behavior appears to be consistent with fungal spore releases [21].

A WIBS-3 instrument was also used in the determination of FAP in the 0.8–20 µm size range at Puy de Dôme, a high-altitude site in France during the summer of 2010. A mean total aerosol concentration of 270 L^{-1}, with a modal size of 2 µm, was observed [120]. The mean fluorescent particle concentration determined in the FL1 channel was 12 L^{-1}, whilst those that were associated with the FL3 channel were found to be 95 L^{-1}. The FL1 channel concentrations did not vary much throughout the campaign, but the FL3 concentrations followed a strong diurnal cycle that peaked at night [21,120].

WIBS-3 and WIBS-4 instruments were also used to characterize bioaerosol emissions from a Colorado pine forest [121]. Both sets of WIBS data were analysed using the previously discussed cluster analysis (*vide supra*) [114,121]. Based on the collected data, all of the fluorescent clusters showed diurnal fluctuations along the forest floor, with minimum concentrations observed at midday (50–100 L^{-1}) and maximum concentrations at night (200–300 L^{-1}) [121]. The cluster behaviours were then compared against those expected for bioaerosols. It was shown that one cluster exhibited the greatest enhancement and highest concentration during sustained wet periods. This behaviour is consistent with that previously reported for fungal spores [22]. A separate cluster dominated the dry periods, which showed characteristics similar to that of bacterial spores [121].

Other notable field measurements include a month long campaign, (August–September 2011) performed at Killarney National Park, Ireland. This work compared the use of two real-time fluorescence instruments, the WIBS-4 and a UV-APS. The results were compared with those obtained from a single-stage particle Hirst-type impactor and standard optical microscopic analysis [98]. Both of the approaches were used to enumerate, categorise, and compare the captured particles/bioaerosols by examining the FAP data in relation to the optical microscopy results. The WIBS and UV-APS showed qualitatively comparable results, with elevated fluorescent bio-particle concentrations at night being noted when maximum RH values and minimum temperatures were measured [98]. Both real-time instruments sampled through the same inlet throughout the campaign, with the mean coarse particle number-concentrations (D_o > 1 µm) measured at 32,800 L^{-1} and 32,400 L^{-1} for WIBS-4 and UV-APS respectively. This observation indicated that there was no significant sampling losses between the instruments [98]. Quantitatively, the two instruments gave results that correlated well with R^2 = 0.90 for the mean total particle concentrations over the campaign [98]. A correlation was clearly observed (integrated number concentrations) between the total biological fungal spore concentrations from the impaction techniques and the WIBS and UV-APS. The fluorescence values of both the instruments showed periodic high and low concentration fluctuations, with concomitant peaks and troughs being measured using optical microscopy occurring at similar time periods as the WIBS-4 FL2 and FL3 channels. However, it should be noted that the FL1 channels bore little temporal similarity [98]. The FL1 channel was dominated by particles with D_o < 2 µm and fluorescent particle concentrations ~10^2 L^{-1} [98]. Such an observation is to be expected since optical microscopy counting is not accurate in this smaller size regime. When comparing the spore number concentrations with each WIBS channel showed R^2 values of 0.05, 0.29, and 0.38 for FL1, FL2, and FL3, respectively. Each of the comparisons suggests that the impaction/optical microscopy method undercounts the WIBS by factors of 3–14× [98]. Finally, it was concluded that the results provided by the three WIBS fluorescence channels provide analytical advantages for bioaerosol classification when compared to the single channel detection approach offered by the UV-APS [98].

During another semi-rural field campaign located in Karlsruhe, Germany, the WIBS FAP concentration data were shown to exhibit seasonal and diurnal variations. Seasonal maximum mean FAP concentrations of 46 L^{-1} were measured in the summer, with a decline in mean FAP concentration of 19 L^{-1} towards winter. The mean FAP concentration over the year was 31 L^{-1} [116]. The contribution of FAP to the total aerosol concentrations again varied throughout the year, being highest in summer (10.6%) and lowest in Winter (3.87%), with a yearly mean of 7.34% (for particles between 0.8–16 μm) [116]. Diurnal FAP concentrations increased after sunset, reaching their highest concentrations during late nights and early mornings. In contrast, total aerosol concentrations were normally highest during the daytime with a decrease noted towards the evening, followed by a sharp decrease after sunset [116]. No correlation was found between FAP concentrations and temperature, precipitation, wind direction, or wind speed. Nevertheless, clear correlations (R^2 = 0.924 and R^2 = 0.911 for spring and summer respectively) were observed between RH and FAP concentrations. The FAP concentrations increased significantly for RH conditions in the 75–95% RH range. However, lower values for the correlation coefficients were observed during both the autumn (R^2 = 0.541) and winter months (R^2 = 0.652) [116].

The varying concentrations of FAP, monitored as a function of altitude, have also been investigated. For example, sampling has been carried out near the surface and subsequently compared to measurements made at 1000 m above ground-level, for a wide range of longitudes across the U.S.A between Florida and California. In this study, a WIBS-4A was utilized to make measurements aboard the airship "Gondola" [113]. FAP counting was recorded for the range between 1–10 μm, revealing particle concentrations, ranging from 2.1–8.7 × 10 particles L^{-1}. These figures are representative of ~24% of the total particle number [113]. Diverse size distributions and distinctive fluorescent characteristics were apparent for these regions. For instance, FAP between 1–4 μm in diameter were observed in the Eastern States which is consistent with the presence of mold spores, whilst larger particles between 3–10 μm diameter were sampled in the Western States, where FAP contributions to the total particle concentration were much more variable [113]. This campaign showed that FAP can contribute significantly to the overall particulates in arid as well as humid environments, and that there are significant sources of bioaerosols in each area, but they may well be of differing types [113].

The fluorescence characteristics of aerosol particles in the polluted atmospheric area of Nanjing, Yangtze River Delta, China has also been investigated [122]. Day-to-day and diurnal variations of FAP were observed and the concentrations were found to be dominated by the FL2 channel, with a mean of 3400 particles L^{-1}, followed by FL3 (2100 L^{-1}) and FL1 (600 L^{-1}). These values are much larger than those found in Amazon (93 L^{-1}), Borneo (150 L^{-1}), and Hyytiälä (23 L^{-1}) [21,57,116], indicating that in the China study, the observed concentrations of FAP were ~1–2× greater. The work also suggests a size dependence for the fractions measured as well as a contribution by diverse FAP types. In the FL3 channel, the 1–2 μm range was reportedly dominated by combustion related particles, with the majority of FAP/biological particles apparent in the 2–5 μm range [122]. A strong correlation (R^2 = 0.75) between FL1 and the $M_{BC}/PM_{0.8}$ (Mass concentration of black carbon/mass concentration of particles in the size range 0.006–0.8 μm) is suggestive of a large contribution from anthropogenic emissions [122]. The high fluorescence values measured, whn combined with the strong correlation between FL1 and $M_{BC}/PM_{0.8}$, suggest that directly using the three fluorescent channels of the WIBS may not be appropriate for indexing PBAP in significantly polluted areas [122].

The WIBS-4A was further used in a study that investigated indoor (office) versus outdoor size-resolved concentrations of fluorescent aerosols. The measurements were undertaken over a period of six continuous days (144 h) in an office located in the campus of Tsinghua University, Beijing, China. The office was 5.1 × 2.7 m^2 in area, 2.8 m high and void of any outside influence i.e., the only indoor source of air was from a filtration system [123]. The WIBS was fitted with an automated control box (KLD2OS 2-way motorised ball valve; Tianjin Kailida Control Technology Development Co., Tianjin, China, allowing for both indoor and outdoor sampling) and a timer device, which permitted the WIBS-4A to switch between indoor and outdoor measurements every 5 min. The results showed

that measurements in the FL1 channel for both indoor and outdoor FAP fitted a bimodal lognormal distribution, with the first peak ranging from 1.35–1.5 μm and the second occurring within the range, 2.1 and 2.25 μm. The R^2 values between indoors and outdoors was 0.938 for the smaller size range and 0.935 for the larger range [123]. A lognormal distribution was also shown to fit the AF dataset, with values for all outdoor and all indoor aerosols peaking at 11–11.5, and a correlation coefficient of $R^2 = 0.992$ being noted between the outdoor and indoor AF values [123]. Linear regression of indoor versus outdoor fluorescent bioaerosol concentrations showed that all of the size ranges from 0.5 to 2.5 μm exhibited very similar profiles with concentrations of indoor and outdoor FAP increasing linearly with respect to each other. However, as particle size increased, the slopes become less steep, possibly reflecting a higher loss rate for larger fluorescent bioaerosols as they enter the building envelope [123]. The time series of the size resolved indoor versus outdoor bioaerosols were also determined using a mass balance equation to model their relationship. Periodic fluctuations throughout all of the size ranges in outdoor non-fluorescent versus fluorescent bioaerosols were also reflected in the indoor concentrations, albeit with a considerable reduction in concentrations, and also with a time lag. Mean concentrations of fluorescent particles made up less than 10% of all the aerosols, leading to similar variations in the non-fluorescent and fluorescent number-concentrations [123].

2.2.3. Ice Nucleation (IN) and Rain Studies

The WIBS has been used for the analysis of PBAP/FAP that is associated with ice nucleating particles (INP) [124–126]. Biologically-derived particles, such as bacteria, have been suggested as plausible sources of INP in certain temperature regimes.

For example, the WIBS-3 has been used to count airborne fungal spores in a semi-arid forest in the southern Rocky Mountains of Colorado. The aim of the study was to measure FAP during wet and dry periods to examine the influence of these spores on mixed-phase clouds, and to investigate the hydrological cycle [91]. The WIBS-3 data, along with UV-APS data, was compared to culture-based spore samplers and off-line molecular tracers for airborne fungal spores. The estimated spore count from the WIBS was within ~13% of the spore count estimated by the tracer method (1.6 to 2.9 × 10 spores L^{-1}) [91]. Similarities between the culture-based sampling and WIBS were also apparent when representative spore counts were measured during the differing ambient conditions. The FAP counts from WIBS showed that they comprised 17–23% of total particle mass during wet conditions, and 2–5% during dry conditions (particle size range 0.8–20 μm). A similar increase of 1.6× between wet and dry conditions was observed using the culture method [91]. Correlations between the fungal molecular tracers mannitol and arabitol, and the WIBS FAP measurements were calculated to be good for both mannitol ($R^2 = 0.8$) and arabitol ($R^2 = 0.82$) during rainy periods [91].

In order to further demonstrate that rain increases the concentrations of airborne FAP/PBAP, and that these closely correlate with ice nuclei (IN) formation in a North American forest, a combination of techniques, including a WIBS-4, was deployed [25]. Statistical cluster analysis of the five particle characteristics that were recorded by the WIBS was then used to confirm that smaller FAP peaked during rainfall events. This behaviour was qualitatively different from that observed for the larger particles, which crested during rainfall, thereby suggesting various particle sources or physiological states [25]. A strong initial enhancement of smaller bio-particles in the range 2–3 μm was observed at the onset of rain events. This period was followed by a less pronounced enhancement during continued rainfall. The behaviour is consistent with the release of bacteria or fungal spores from surrounding vegetation surfaces via mechanical agitation with rain drops [25]. Larger bio-particles (4–6 μm in size) were shown to contribute to the local environment during the humid post-rain period. Again, this behaviour is consistent with the observed upward flux of fluorescent bio-particle emission after rainfall events (~50–500 m^{-2} s^{-1}). It has been suggested that the enhanced WIBS signals coincide with freshly emitted bio-particles that were growing on wetted earthy surfaces near the measurement site [25]. A large and closely correlated upsurge in bio-particles and IN was observed throughout the rain events. These rain-enhanced bio-particles and ice nucleating particles (INP) were active in what

is considered the warmest regime of mixed-phase clouds (≥ -15 °C), which is also a regime that is normally associated with biological particles [25].

A WIBS-4A has been used to measure fluorescent bioaerosol particles at temperatures that are associated with the formation of mixed-phase and cirrus clouds by deployment on board the National Centre for Atmospheric Research (NCAR) Gulfstream V aircraft. The WIBS data collected was used to develop the lower (particles fluorescent in both A and C channel) and upper bounds (all categories of particles fluorescent in the A or C channel) of FBAP concentration, which was reliant on fluorescent response. A trend was observed, whereby the concentration of FAP in the size range between 0.8 and 12 µm in diameter decreased with altitude. Generally, the FAP concentrations were found to be between 10 and 100 L^{-1} in the continental boundary layer, but always decreased significantly to 0–1 L^{-1} at temperatures that were lower than 255 K in the free troposphere [127]. The highest variability of the FAP was observed at temperatures where biological INP could influence mixed-phase cloud formation (255 K $\leq$ T $\leq$ 270 K). The 2–5 km altitude range coincides with temperatures where mineral dusts are less active as INP. These observations potentially indicate that INP of a biological origin are critical to mixed-phase cloud formation [127]. Particle size was also measured and the mode size of the FAP was determined to be ~2–3 µm. This range is consistent with the previous studies discussed above [25]. The mean percentage of particles in the range 0.8–12 µm that fluoresced in the lower bounds was 3%, and in the upper bounds was 11%, which, again, is consistent with other reports [128].

2.2.4. Occupational Site Campaigns

Recently, the WIBS-4 has been deployed for the first time to detect bio-aerosol emissions and non-fluorescing "dust" released from a composting/green waste site at a remote rural location (~6 km due north of the Irish coastline). The overall campaign was carried out for a seven-day period between 30th of September and 17th of October 2014 [129]. Three short term visits were undertaken, two during weekdays and one at the weekend when the site was formally closed. The weekday campaigns were categorised by the site manager in terms of workload: one as a "light" workload period and the second as a "heavy" workload period. Each campaign measured four different FAP profiles: (a) Size (µm) vs. Time (h) fluorescent number-concentration plots; (b) AF value ("shape") vs. time (h) fluorescent number-concentration plots; (c) Wind rose graphics for fluorescent number-concentrations with wind speed and direction; and, (d) Effect of relative humidity on fluorescent number counts [129]. The data collected showed that the FAP measurements for all three campaigns accumulated in one principle size regime (~0.5 µm to ~3 µm). The non-fluorescent "dust" exhibited a smaller size regime (~0.5 µm to ~1.5 µm). Over the entire "light" working day, the average fluorescent proportion of total particles counted was ~1% (FAP = 109.9 particles L^{-1}). On the "heavy" working day, the average fluorescent proportion of total particles counted was ~7% (FAP = 304.2 Particles L^{-1}) and at the weekend, the average fluorescent proportion of total particles counted was ~18% (FAP = 320.2 Particles L^{-1}) [129]. It was noted that far fewer particles were collected at the weekend (particles sizes between 0.5–13 µm). The profile results for the site showed that FAP counts vary significantly depending on working activity, time of day, and local weather conditions e.g., wind speed [129].

Table 4. Comparison between results of studies utilizing various models of the WIBS instrument. Equivalent Optical Diameter (EOD) is recorded in the µm size range. Number-concentrations of fluorescent aerosol particles (FAP) is reported in L^{-1}. (Numbers in parentheses are the fraction of fluorescent particles from the total particles collected as a %).

Site Location	WIBS Model	Site Category	Season	EOD Range	N_{FL1}	N_{FL2}	N_{FL3}	N_{FAP}	References
Manchester, England	3	Urban	Winter	0.8–20	29 (3%)	52 (6%)	110 (11%)	-	[21]
Borneo, Malaysia	3	Rainforest	Summer	0.8–20	-	-	-	150	[21]

Table 4. *Cont.*

Site Location	WIBS Model	Site Category	Season	EOD Range	N_{FL1}	N_{FL2}	N_{FL3}	N_{FAP}	References
Puy de Dôme mountain, France	3	High-altitude	Summer	0.8–20	12 (4.4%)	-	95 (35.2%)	-	[120]
Cork, Ireland	4	Coastal	Summer	3.0–31	~25	~11	~2	(~15%)	[22]
Killarney, Ireland	4	Rural	Summer	0.5–13	-	-	-	-	[98]
Karlsruhe, Germany	4	Semi-rural	1-Year	0.8–16	-	-	-	31 (7.3%)	[116]
Southern USA	4	High-altitude	Autumn	1.0–10	-	-	-	(24%)	[113]
Jungfrau, Switzerland	4	High-altitude	Winter	>0.8	-	-	-	6.3 ± 5.7	[130]
Nanjing, China	4a	Suburban	Autumn	1.0–15	570 (4.6%)	3350 (25.3%)	2090 (15.6%)	-	[122]
Vancouver, Canada	4a	Coastal	Autumn	0.5–10	-	-	-	(7.8%)	[14]
Colorado, USA	3/4	Rural Forest	1-Year	0.8–20	-	-	-	(7.12%)/ (4.02%)	[121]
North Carolina, USA	4a	Urban	Autumn	0.5–15	-	-	-	(41.63%)	[131]
Denver, USA	4a	High-altitude	Autumn	0.8–12	-	-	-	69 (11%)	[127]
Nanyang, Singapore	4a	Indoor	-	1.0–10	-	-	-	(~50%)	[118]
Beijing, China	4a	Indoor	Spring	0.5–10	-	-	-	(4.37%)	[123]
Beijing, China	4a	Urban	Winter	>0.8	155 (3.3%)	551 (11.4%)	79.4 (1.5%)	642 (13.3%)	[132]

2.3. BioScout

BioScout is an optical LIF real-time bioaerosol system developed at TUT (Tampere University of Technology), before being commercialized by Environics Ltd. [133]. The BioScout unit utilises a 405 nm continuous wave laser diode operating at 200 mW optical power, to induce autofluorescence from individual bio-particles. The autofluorescence and the scattered light are collected via an elliptical mirror, before being separated using a beam-splitter and focused onto two photomultiplier tubes (PMTs). The scattered light is then used to examine the optical particle size, whilst the autofluorescence is isolated from the scattered light using a 442 nm long-pass filter prior to detection at the PMT. The fluorescence intensity is then organised into sixteen intensity channels. The BioScout manufacturers specify a working particle size analysis range from 0.5–10 µm and a time resolution of 1 s. Newer models of the BioScout also include an additional functionality, enabling secondary air sampling of bio-aerosols using filter substrates, which can then be used for subsequent biological analysis.

The BioScout has been comparatively tested against the well-studied Ultraviolet Aerodynamic Particle Sizer (UV-APS), under both laboratory conditions and in field campaigns. The laboratory results of an initial study indicated that the BioScout had a higher fluorescent particle detection efficiency for aerosolized fungal spores (*Aspergillus versicolor*, *Penicillium brevicompactum*, and *Penicillium expansum*), aerosolized bacterial spores (*Bacillus atrophaeus* and *Bacillus thuringiensis*), and the common biochemicals (ovalbumin, tryptophan, and riboflavin) when compared to the UV-APS system [133]. The authors speculate that the higher fluorescent particle fraction (FPF) values observed with the BioScout are due to its more powerful laser, when compared to the UV-APS system. They also note the possibility that the variation of detectors and emission bands that are utilised within each system, might also contribute to the observed difference in fluorescence sensitivity (405 nm excitation for the BioScout and 355 nm excitation for the UV-APS). The UV-APS did however fare better with biochemical particle analysis of NADH, with substantially higher fluorescent particle fraction (FPF) values being observed when compared to the BioScout. The higher FPF values observed for NADH when monitoring using the UV-APS, were attributed to the near coincidence of the excitation peak of NADH with that of the UV-APS 355 nm laser line [62]. When examining the particle size responses of each instrument, the study noted that the UV-APS appeared to possess better size resolution, whereas the BioScout appeared to demonstrate more efficient particle counting with smaller particle sizes. Discretion is required when making such comparisons since the two instruments use differing

measurement modalities. The UV-APS measures the aerodynamic diameter of particles, whilst the BioScout measures optical diameter, which is dependent on the optical properties of the particles.

A second laboratory study also compared the UV-APS and BioScout systems when examining the fluorescent properties of aerosolized fungal spores. Comparisons between instruments were made as a function of the fungal species under examination (*Aspergillus versicolor*, *Cladosporium cladosporioides* and *Penicillium brevicompactum*), their cultivation time, growth substrate and the air exposure velocity [134]. The study concluded that all of these factors had an impact on the detection efficiency of fungal spores when utilising fluorescence-based systems. When the two systems were compared, the difference in the observed FPF values were less striking than the previous study, and were found to be broadly comparable for both instruments. However, in two cases, the age of two spore varieties led to statistically significant differences in the compared FPF values. The FPF values that were observed with the BioScout were higher (in the case of four-month-old *A. versicolor*) and lower (in the case of four-month-old *P. brevicompactum*) when compared to the UV-APS. The authors attributed these FPF variations between the two systems to the differing fluorescent compounds produced within late stage *Aspergillus versicolor* and *Penicillium brevicompactum* spores, coupled with the dissimilar excitation wavelengths used within each system.

The BioScout and a UV-APS system were also compared in a study involving a summer and winter measurement campaign examining fluorescent aerosol particles (FAP) and size distributions in suburban and urbans sites in the Helsinki metropolitan area, Finland [96]. Two FAP modes were detected during the summer period at 0.5–1.5 μm (fine) and 1.5–5 μm (coarse). The results showed a high correlation between the instruments for the total particle count for both modes, in spite of the different modalities utilised for their measurement (*vide supra*). Comparison of the UV-APS and BioScout FAP detection efficiencies also suggested that the BioScout demonstrated 2.6× and 9.7× higher detection efficiencies for the coarse and fine modes, respectively. Again, the authors attributed the observed efficiencies to the higher laser intensity of the BioScout and the good signal to noise ratio of the fluorescence signal that is associated with the system.

Overall, given the observed FAP detection efficiencies that are associated with the use of the 405 nm excitation line within the BioScout system, and notwithstanding the line's relative insensitivity to NADH, it appears that this excitation wavelength may prove interesting in the continued development of instrumentation for the real-time detection of airborne microorganisms [133].

3. Overview of the Use of Real-Time Bioaerosol Detectors

Over the past two decades, there has been a steady increase in the number of published peer-reviewed manuscripts incorporating the real-time fluorescent monitors outlined in this review (Figure 1). This information signifies the increasing normalization and integration of real-time bioaerosol sampling in ambient air monitoring campaigns.

From Figure 1 it can be seen that towards the beginning of this century there was limited research published in the area and that data was almost exclusively obtained by the use of UV-APS (red). However, as time progressed, not only have the overall number of papers increased, but a far larger proportion have included the use of the WIBS instrument (blue). Relatively few studies have been undertaken using the BioScout (green), but it should be noted that this instrument was not developed and deployed until more recently.

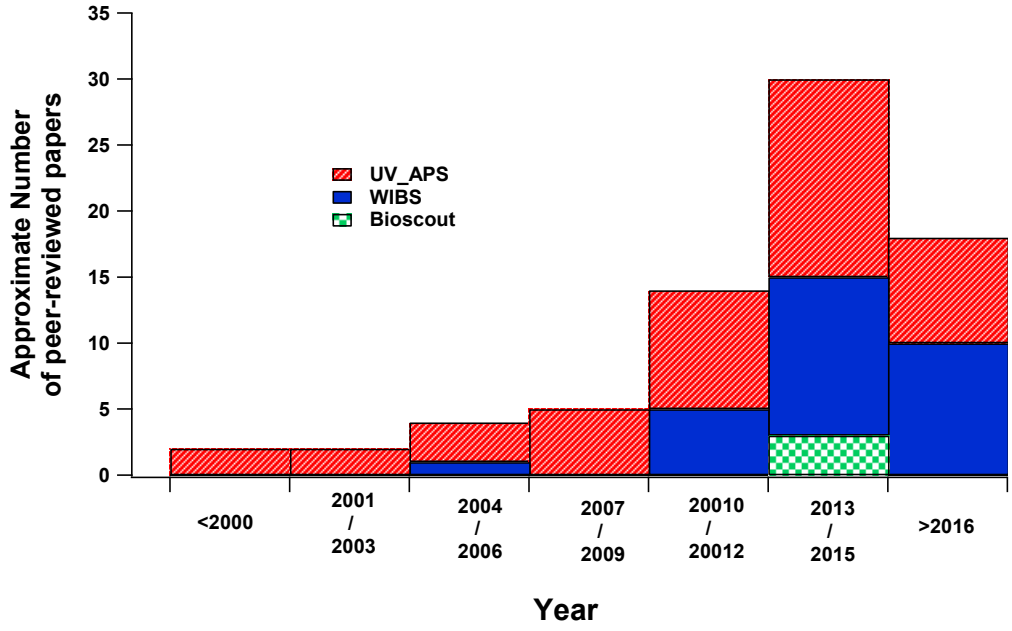

Figure 1. Indicates the increase in the number of peer reviewed manuscripts published over the last 20 years that have employed real-time fluorescent particle instrumentation for detection.

In tandem with increasing numbers of publications, the area has seen a growth in the geographical spread of sampling campaigns, and the number of research groups utilizing the techniques (Figure 2). The diversity of the site environments that are used for deployment is now more extensive with rural, coastal, high-altitude, tropical forest, urban, mega-cities, and laboratories all noted in the literature. China in particular has seen a steep rise in the number of campaigns undertaken. This may provide opportunities to better assess the performance of real-time fluorescent instrumentation under conditions of significant and sustained air pollution levels [135]. It is also interesting that large swathes of the globe remain unexplored with respect to real-time bioaerosol analysis. In particular, potentially useful studies that are assessing long range transport of fungal spores and other PBAP to areas, such as Greenland and Antarctica, remain unexamined.

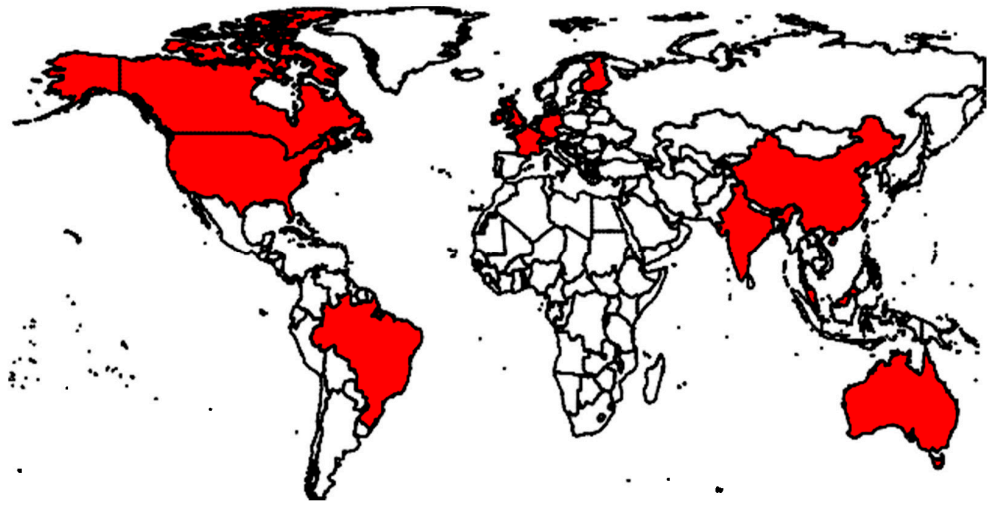

Figure 2. Map of the world with the red regions representing countries where the real-time fluorescent particle instrumentation (UV-APS, WIBS and BioScout) reviewed have been deployed.

Figure 3 highlights the results obtained from selected location types (as defined by the authors) sampled using the real-time techniques. Upon examination of the collated data, it is clear that the "Polluted" locations appear to have the greatest concentration of fluorescent particles, although care must be taken when interpreting this data since relatively few campaigns in these environments have been performed to date. Given the preponderance of ambient non-biological interferents associated with polluted environments, it is unlikely that all of the sampled fluorescent particles were biological in nature, so a degree of care must be taken with respect to interpretation due to possible PBAP false positives. However, even with the presence of significant levels of interferents, the data can still yield important information to atmospheric scientists and epidemiologists due to the adverse health effects of the fluorescent chemical particles that are associated with high levels of SOA. Similarly to "Polluted" locations, few sampling campaigns have been carried out at "High-Altitude" sites and a full characterization of their fluorescent particle loading is not currently available.

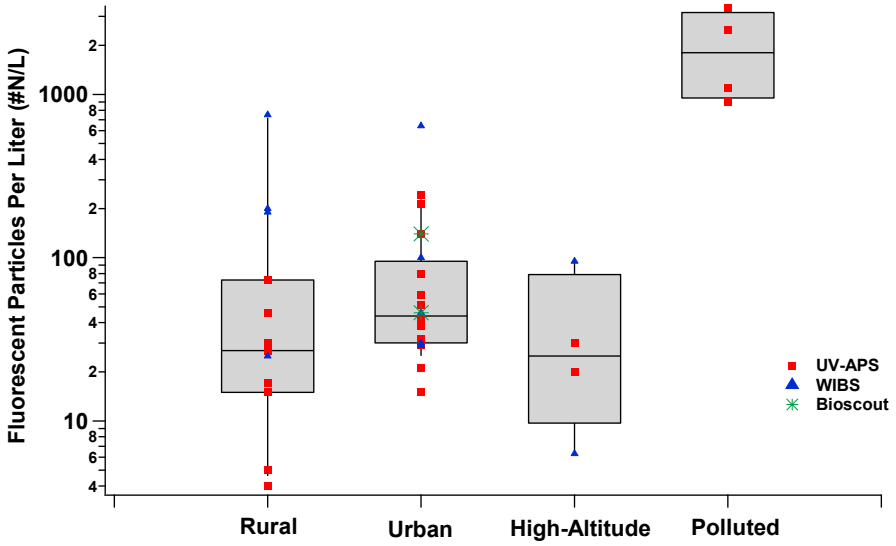

Figure 3. Mean number of fluorescent particles per liter counted for selected ambient environments. (Squares indicate values sampled using the UV-APS, triangles for WIBS and stars for the BioScout). The grey box plot and whiskers indicate the 10th, 25th, 50th, 75th, and 90th percentiles for the data.

As is suspected, although not being explicitly proven to date, the measurements that are made in urban settings return a higher median concentration value of fluorescent particles when compared to those that are found in rural settings. This finding is likely due to the increased concentration of interfering chemical particles at the "Urban" sites when compared to "Rural" sites. Of statistical note, all of the locations described as an "Urban" setting display the tightest interquartile range of 60 particles/L when compared to 65 particles/L and 80 particles/L for "Rural" and "High-Altitude", respectively. It is also clear from the data that seasonal trends tend to affect the concentrations of fluorescent particles that are monitored at rural and urban locations. Hence, winter, autumn, and spring levels were seen to be far lower than summer values at rural locations.

The seasonal breakdown for the fluorescent particle concentrations is shown in Figure 4. Differing trends are clearly apparent between the rural and urban settings. The graphic shows that winter values in urban areas are larger than those that are recorded at any other time of the year. This, again, is not surprising, but has not been quantified hitherto. The winter times generally coincide with an increased use of domestic heating (especially the burning of solid fuels), which is likely to lead to enhanced numbers of interfering fluorescent SOA particles in such environments. The reason for the contrasting data obtained during winter periods for rural sites is probably due to the lower density of housing in these rural locations. Furthermore, weather conditions, such as snow, cold, and sustained

rain can also hinder the release of biological particles. These conditions are more prevalent during winter and can depress the growth and reproductive cycles of flora, and lead to lower concentrations of biological particles. The plot also confirms that the highest average concentrations of fluorescent particles that are measured at rural environments are during the summer season. The high "Rural" summer average was seen to be almost a factor of 10× larger than those seen during any other seasonal period.

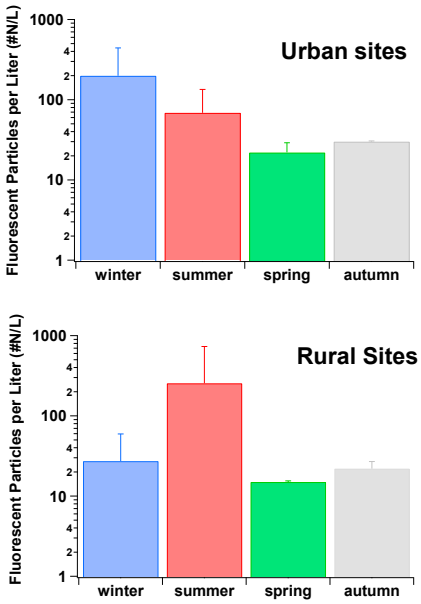

Figure 4. Mean fluorescent particle concentrations measured as a function of site location and temporal period using the UV-APS, WIBS, and BioScout instrumentation.

Another interesting observation is the percentage of both fluorescent and non-fluorescent particles (>1 µm) sampled in both "Rural" and "Urban" settings, as shown in Figure 5.

This plot suggests that the fraction of fluorescent particles is lower by a factor of ~50%, in "Urban" locations when compared to the "Rural" settings. This information is of interest as the fluorescent particle number concentrations that are shown in Figure 5 are higher for "Urban" settings than they are for "Rural" settings.

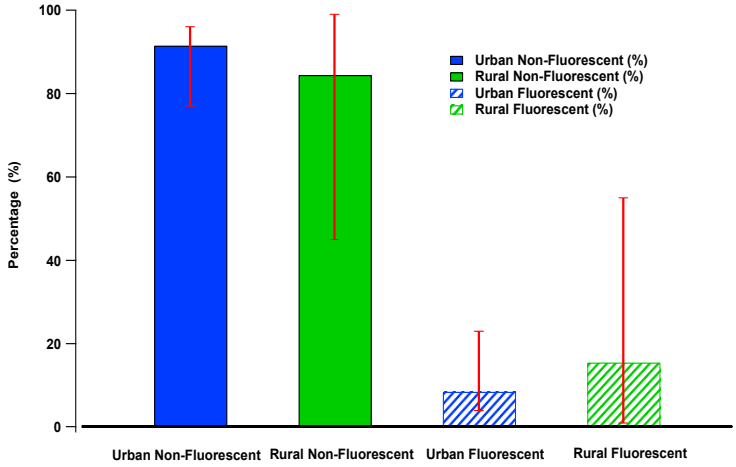

Figure 5. Fluorescent and non-fluorescent fractions of the total particle concentrations for particles >1 µm in urban and rural locations (error bars reflect maximum and minimum values).

4. Intercomparisons of the Real-Time Fluorescence Devices

This section of the review, will seek to comparatively examine the reviewed real-time fluorescence bioaerosol instruments by summarizing intercomparison campaigns that have been undertaken in field and laboratory settings.

Table 5 below outlines the operational parameters of each of the instruments. The most readily apparent observation is the variety of excitation sources that are used by the instruments with both the UV-APS and BioScout favoring lasers, while the WIBS utilizes multiple flash lamps. The devices all use an excitation wavelength between 370–405 nm (to coincide with NAD(P)H and flavin light absorption maxima amongst others), the WIBS also exploits a shorter wavelength excitation source to discriminate between particles. The 280 nm wavelength flash lamp was included as it provides the required wavelength to excite amino acids, which are constituents of all the biological particles. This additional wavelength facility is absent in the other instruments, which may reduce their ability to detect certain fluorescing particle types. Several laboratory experiments using the WIBS and bacteria have highlighted the importance of the 280 nm wavelength (Channel A or FL1) for bacterial detection. In these studies, aerosolized bacterial samples were observed to fluoresce almost exclusively in channel A (with little if any fluorescence noted in the other detection channels) [117].

Table 5. Specifications of the online real-time devices.

Device	WIBS-4/4A	UV-APS	Bio-Scout
Excitation (nm) and/or scatter source	280/370 nm (two Xe flashlamps)	355-nm UV laser (30 mJ)	405 nm laser diode
Fluorescence detection range	310–400 nm and 420–650 nm	430–580 nm	>442 nm
Size detection range (μm)	0.5–12 HG; 3–30 LG (WIBS-4) or 0.5–20 μm (WIBS-4A)	0.5–20 μm	0.5–10 μm
Time resolution	Millisecond	1 s–18 h (5 min generally)	1 s
Sample flow	0.24 L/min (WIBS-4); 0.3 L/min (WIBS-4A)	1 L/min	2 L/min
Total flow	2.4 L/min (WIBS-4); 2.5/0.3 L/min (WIBS-4A)	5 L/min	2 L/min

Both the UV-APS and the BioScout have also been used to detect bacteria in a laboratory setting. In one study, both instruments were subjected in parallel to a variety of test aerosols in order to ascertain their fluorescent particle fraction (FPF). The aerosols used varied from bacteria to a number of dispersed bio-chemicals. In the majority of cases, the BioScout described a greater fraction of the aerosols as fluorescent. Overall, the BioScout FPF values varied between 0.34–0.77 for single bacterial spores, while the UV-APS FPF values for the bacterial spores were significantly lower (between 0.13–0.17). Interestingly, smaller particles of the same particle type comprised lower fluorescent fractions of the total. These results suggest that these particles did not produce sufficient fluorescence emission to enable their detection by the instruments, and were thus below the instrument detection limit, rather than being non-fluorescent in nature. However, the UV-APS did return far higher fluorescent fractions for the bio-chemical NAD(P)H. This finding was not surprising given the 355 nm laser used by the UV-APS excites in the excitation range (340–366 nm) of NAD(P)H, whereas the BioScout laser does not (405 nm). Thus, this study suggests that the BioScout is potentially more sensitive than the UV-APS for the detection of bacterial cells, but the ability of the UV-APS to induce NAD(P)H fluorescence may prove to be of greater interest in the detection of viable or metabolically active biological particles [133].

Other laboratory studies have shown that the UV-APS can detect fluorescence from individual bacterial cells (*B. subtilis*), however, very little fluorescence from bacterial endospores was noted [83]. To explain their results, the authors suggested that bacterial endospores are dormant (i.e., lack metabolic activity), and therefore do not contain sufficient concentrations of NAD(P)H to elicit a response above the instrumental sensitivity threshold.

The second excitation channel incorporated into the WIBS may also allow for the enhanced detection of fungal spores in comparison to the other instruments. As was observed for bacteria samples, several laboratory studies have also shown that fluorescence channel A is the most likely to characterize fungal spores [99,117]. One study showed that for a particular fungal spore species tested ~80% of the fungal spore numbers could be characterized as "A-type" particles [117]. This specific information cannot be obtained using the UV-APS or the BioScout due to their inability to excite particles at 280 nm. However, laboratory studies have shown that while the UV-APS and the BioScout can detect fungal spores [61,82,134] (implying other excitation wavelengths and detection bands are still useful), the question as to what fraction of the total fungal spore concentration they sample in comparison to the WIBS has not been answered.

Parallel sampling of the aforementioned instruments during field studies has also allowed for the direct comparison of their capabilities. For instance, the BioScout and the UV-APS have been the subject of a comparative study in an urban environment [133]. Both of the instruments correlated well for fluorescent particles >1.5 µm (R = 0.83) and <1.5 µm (R = 0.92). One significant difference noted was the concentration of fluorescent particles that were sampled with the BioScout, which showed 2.6× and 9.7× values for the coarse and fine FAP, respectively [96]. Similarly, the WIBS and the UV-APS have been stationed together during a field campaign in Killarney Ireland. Importantly, both returned virtually identical total particle concentrations, implying that total particle counts obtained for both instruments may considered as equivalent. Furthermore, the FL3 channel intensities obtained with the WIBS correlated well with the UV-APS fluorescent counts. In contrast, the WIBS FL3 counts were measured to be far higher than those provided by the UV-APS (by a factor of ~2). In this study, the WIBS instrumental data led to a bi-modal distribution of particle sizes at ~3–4 and ~1–2 µm. This distribution was not observed using the UV-APS, with only the larger mode being registered. This sizing result possibly indicates that the WIBS approach is more suited for the detection bacteria when compared to the UV-APS. Collections from both of the instruments were positively correlated with those that were obtained using traditional impaction/optical microscopy methodologies. This important feature has been subsequently confirmed for WIBS and traditional measurements at a number of locations [32]. Real-time instrumentation tends to return larger concentration values than those that are obtained using a traditional sampler [32]. This finding is most likely due to the poor collection efficiencies of the traditional samplers, coupled with operator error when counting large concentrations by eye. WIBS results also correlate well with those obtained from fungal spore tracer methods [91]. For example it has been found that WIBS results were within ~13% of the spore count estimated by a tracer method. The UV-APS approach has also been contrasted with off-line sampling methods (e.g., AGI-30 impingers) and the studies have shown good agreement [82].

The capability of each instrument to evaluate particulate size ranges also varies. The WIBS and the UV-APS can effectively sample larger biological particles (>20 µm depending on the version and instrument), whereas the BioScout size range cut-off size is 10 µm, and therefore precludes it from the detection of larger fungal spores and pollen. The WIBS instrument is the only reviewed instrument that has been successfully used to detect pollen in both laboratory and outdoor environments. In addition, the instrument has been shown to respond to a host of different fungal spores and pollen grains in terms of fluorescence signals, sizing, and asymmetry factors, but PBAP identification at the species level still remains elusive.

Finally, the flow rates of the three instruments differ significantly (Table 5). The UV-APS with its 5 L/min flow rate is the largest of the three, which provides advantages to ambient outdoor sampling as vertical sampling lines are generally used. This feature allows for more effective sampling of fast-moving particles during windy periods.

5. Future Instrumental Developments

Newer instrumental techniques based on the premise of single particle fluorescence continue to be developed. These instruments offer greater sensitivity and even the prospect of spectrally

resolved fluorescence spectra. Among the most promising instruments are the Particle Analyser PA-300, the Spectral Intensity Bioaerosol Sensor (SIBS), and the Multi-parameter Bioaerosol Sensor (MBS), manufactured by Plair SA, Droplet Measurement Technologies, and the University of Hertfordshire/DSTL, respectively. These instruments and their operational parameters can be seen in Table 6 below. In principle, these instruments function similarly to those discussed above. However, such devices are designed to give additional information over the full fluorescence emission wavelength ranges to aid with actual identification of the FAP/PBAP by essentially determining the individual spectroscopic "fingerprints" for specific biological species. An overview of each instrument is given below. Although they are all commercially available, there are little or no peer reviewed publications to confirm their capabilities as of yet.

5.1. PA-300

This instrument is based on the work of Kiselev et al. [136,137] and uses both optical scatter and spectrally resolved fluorescence for the identification of biological particles by providing a near complete spectrum for each particle. The instrument has an air-flow rate of 2 L min^{-1}, and initially passes particles through a red laser beam (658 nm) to yield time-resolved scattering data. The signals are recorded by two photo-detectors that also characterize the optical shape, size, and surface properties. The manufacturers claim that the instrument can measure particles in the size range of 1–100 µm, which represents a far larger span than any of the instrumentation described above. Subsequent to the initial laser excitation, a second laser beam (377 nm) excites the particles and the resultant fluorescence signals are recorded using a diffraction grating and an array of 32 photo-detectors (32 equal bins with overall range 390–600 nm). Again, the span is far greater than the instruments mentioned hitherto. Additionally, and unique to the PA-300, the phosphorescence of individual particles can also be recorded. This will allow for the further investigation of the intrinsic photophysical properties of biological particles, and possibly aid in the discrimination between biological species.

Only one peer-reviewed publication is currently available on the use of the PA-300 [138], which sought to analyze the performance of the PA-300 with regard to pollen identification and airborne particle concentrations. The spectral measurements were made in parallel to a manual reference measurement instrument (Hirst-type volumetric sampler/optical microscopy) during a Swiss pollen season (14th February–31st August, 2016). The studies were made at the MeteoSwiss site in Payerne, Switzerland. The PA-300 that was used on this campaign was modified to provide an inlet system, which increased the factory standard sampling levels. A concentrator provided by Plair SA and based on the virtual impactor principle, was also used in conjunction with a second pump (flow rate 30 L min^{-1}). A good correlation between the expected and measured values (r = 0.88) was calculated when comparing 16 different pollen types. To simplify the pollen counting process, only particles fluorescing between 390 nm and 600 nm and with sizes <9 µm were analyzed. The PA-300 measurements recorded ~25 times more events than the manual sampling approach. There was a high correlation between the two methodologies (r = 0.95) for total pollen counts. This trend was also noted for individual species, such as grass pollen (r = 0.83), amongst others. These observations are of great interest given that grass pollen is generally considered to be the greatest contributor to hay fever [138]. Recently, an extended version of the PA-300 has been developed, the PA-1000. It has enhanced capabilities for the detection of aerosols down to 0.5 µm. The PA-1000 can also provide time-resolved excited state lifetimes of individual particles. This has the potential to provide an additional intrinsic physical property with which to discriminate between particles possessing similar physical and spectral characteristics. Previous work has demonstrated that individual particles can be discriminated on the basis of their excited state lifetimes, albeit in an off-line capacity. A study by O'Connor et al. (2014) [36] showed that different species of pollen returned different lifetime values based on their photophysical properties [36].

However, there are currently no peer reviewed reports that are available documenting its use.

5.2. WIBS-4+ and WIBS-Neo

During a laboratory study that measured the fluorescence spectra and the lifetimes of individual pollen grains, the biomolecule chlorophyll-a was shown to be a possible biomarker for grass pollen due to its unique fluorescence peak at 670 nm [36]. It is suggested that this biomarker could be used to specifically characterize grass pollen, as opposed to tree pollen, which does not give rise to the same signal [36]. Therefore, to specifically detect chlorophyll-a fluorescence, an upgrade of the WIBS-4 was developed and termed the WIBS-4+. This instrument provides two additional fluorescence data channels, FL4 and FL5. The FL4 signals derive from the excitation of particles at 280 nm, while FL5 signals come from the excitation of particles at 370 nm. Potential emission from chlorophyll-a is recorded by a photomultiplier in the 600–750 nm range. The WIBS-Neo is conceptually the same as the WIBS-4A, but incorporates a working particle size range of 0.5–50 µm, has improved sensitivity and the capability of measuring fluorescence lifetimes. However, no peer-reviewed papers are available on either the WIBS-4+ or the WIBS-Neo as of this time.

5.3. Multiparameter Bioaerosol *Spectrometer (MBS)*

Although being the first of the next generation of real-time techniques for airborne PBAP/FAP analysis to be developed, there is only one peer-reviewed publication that reports the use of an MBS [139]. The MBS is an evolution of the WIBS technology and provides data relating to the size (1–20 microns), shape, and autofluorescence of individual airborne particles. However, where the WIBS-3 and WIBS-4(A) only record particle fluorescence over two ranges, 310–400 nm and 420–650 nm, the MBS provides spectral distribution histograms over eight wavelength bands: 300–335 nm, 340–385 nm, 390–435 nm, 440–485 nm, 490–535 nm, 540–575 nm, 580–615 nm, and 620–655 nm. The end-result is comparable to a traditional spectrum because individual fluorescing particles give rise to specific spectral distributions. When combined with the ability to determine FAP size and shape using an arrangement of two 512-pixel CMOS detector arrays to record high-resolution data, improved discrimination between biological and non-biological particles would appear to be possible with this instrument arrangement [139].

The MBS operates by drawing ambient aerosol at a rate of ~1.5 L min^{-1} through an inlet tube before being split. Parts of this flow are then used as both a "bleed flow" (to maintain inner optical chamber cleanliness) and as a "sheath flow" to surround and direct the remaining 300 mL min^{-1} sample flow. Particles that are confined in this sample flow are forced through the so-called "sensing volume", which is the juncture between the particle detection laser beam and the sample airflow column. Here, individual particles are first irradiated by a low-power laser beam (12 mW at 635 nm) and the subsequent light scatter from the laser pulse is collected by a lens assembly, while a small proportion of this light is directed by a pellicle beam splitter to a photodiode trigger detector. The voltage output pulse of this detector is proportional to the light intensity and is used to determine particle size. The trigger detector signal also induces the firing of a second, high-power pulsed laser (250 mW at 635 nm) to irradiate the particle with sufficient intensity to allow two CMOS linear detector arrays to then capture the morphology and orientation elements associated with spatial light scattering pattern of the particle. About 10 µs after particle detection, an intense UV pulse (at 280 nm) illuminates the particle for ~1 µs, resulting in fluorescence of the analyte particles. The fluorescence is then focused onto the spectrometer optics. The eight channel PMT records a fluorescence spectrum between 310–650 nm after which the electronics control unit (ECU) digitizes and documents the information. The particle then exits the chamber and the process is repeated for further particles. The total time taken to measure one particle is 30 µs, meaning that the system has the potential to count particles at a rate greater than 1000 particles per second. However, the xenon lamp has a recharge time of ~5 ms, which then becomes a limiting factor, and reduces the data collection rate to ~100 particles s^{-1} equivalent to 2×10^4 particles L^{-1} [139].

5.4. SIBS

SIBS is also based on the WIBS instrument design and uses several identical components. However, like the MBS, it provides additional spectral information by recording 32 combined channels of fluorescence intensity per particle. It also has the ability to determine fluorescence lifetimes of particles. The SIBS measures particles with sizes in the lower sub-micron range ($\geq$ 0.1 µm). No peer-reviewed publications are yet available regarding the use and efficacy of this technique in either field or laboratory settings.

6. Caveat to New Instrumental Developments

The current limitations associated with all of the newer devices are not those of hardware, but rather of software design due to the increased number of detection channels giving rise to greatly increased data sets. Dealing with these large sets of "big data" requires not only the application of sophisticated statistical methods, but also the development of appropriate software packages. Improving the ease-of-use and the general accessibility of the necessary data-handling packages must become a top priority for the bioaerosol community.

Table 6. Comparison between reported instrumental parameters of future instrumentation.

Parameter	PA-300	PA-1000	MBS	WIBS-4+	WIBS-Neo	SIBS
Excitation source	337 nm UV-laser beam	263 nm UV-laser beam	280 nm Xenon flashtubes	280 and 370 nm Xenon flashtubes	280 and 370 nm Xenon flashtubes	280 and 370 nm Xenon flashtubes
Aerosol sampling flow rate	2.0 L min^{-1}	2.8 L min^{-1}	0.30 L min^{-1}	0.30 L min^{-1}	0.30 L min^{-1}	0.30 L min^{-1}
Sizing method	Optical Diameter (D_o) by Mie theory	Optical Diameter (D_o) by Mie theory	Optical Diameter (D_o) by Mie theory	Optical Diameter (D_o) by Mie theory	Optical Diameter (D_o) by Mie theory	Optical Diameter (D_o) by Mie theory
Particle size range	1–100 µm	0.5–100 µm	1–20 µm	High-Gain = 0.5–12 µm Low-Gain = 3–31 µm	0.5–50 µm	N/A
Fluorescence	32 equal bins between 390–600 nm	32 equal bins between range 290–660 nm	300–335 nm, 340–385 nm, 390–435 nm, 440–485 nm, 490-535 nm, 540–575 nm, 580–615 nm, 620–655 nm	FL1 λ_{ex} = 280 nm, λ_{em} = 310–400 nm FL2 λ_{ex} = 280 nm λ_{em} = 420–650 nm FL3 λ_{ex} = 370 nm λ_{em} = 420–650 nm FL4 λ_{ex} = 280 nm λ_{em} = 600–750 nm FL5 λ_{ex} = 370 nm λ_{em} = 600–750 nm	FL1 λ_{ex} = 280 nm, λ_{em} = 310–400 nm FL2 λ_{ex} = 280 nm λ_{em} = 420–650 nm FL3 λ_{ex} = 370 nm λ_{em} = 420–650 nm	16 channels between 300–720 nm

7. Conclusions

The area of real-time PBAP sensing is an area of continued and sustained research interest. This review sought to illustrate the considerable body of work that has already been published in the area of real-time PBAP sensing by collating studies, which demonstrate the wide array of locations, applications, and potential uses for such instrumentation. As the efficiency and sophistication of such devices has increased in tandem with advances in the interpretation and analysis of the collected data, it is clear that real-time sensing of PBAP now represents a significant pillar in the current edifice of PBAP evaluation methodologies. This is evidenced by the number of studies throughout the review that highlighted the correlation between real-time devices and other off-line instrumentation, thus emphasizing their ability to capture similar information, albeit at much higher resolutions. However, the review also notes that these instruments do suffer limitations, especially when deployed within environments with significant SOA concentrations, such as those that are found in heavily polluted urban areas. Other interfering species were also noted in the review and possible methodologies for the limiting of false positives were discussed. The increased functionality of the next generation of instrument also promises great strides not just in the quantitation of PBAP, but also crucially in their identification. One very interesting development is the possibility of assessing the

aggregate excited state lifetimes of individual particles, which should lead to even greater selectivity when analyzing atmospherically relevant biological species. These measurements could lead to the development of potential "finger print" signals, which could greatly aid in the differentiation of physically and spectrally similar bio-particles, on the basis of their disparate excited state lifetimes. As discussed in the review, the possible influence of PBAP on ice-nucleation is an area of increased interest, which requires not just concentration data, but also this strong qualitative information on the particular PBAP implicated in IN processes. As such, further advances in this area of instrument development are expected to garner significant interest in this field. As further demonstrated by the outlined literature, real-time PBAP data can be readily studied with reference to meteorological parameters in order to model the attendant releases of biological particles. It is expected that pollen forecasting in particular could benefit from the enhanced real-time monitoring capabilities of such devices. The new instrument developments also provide the potential for these monitors to be routinely utilized as real-time bio-particle alarms. This could significantly aid in the protection of workers within environments that potentially generate hazardous concentrations of PBAP e.g., agricultural, composting, and waste water treatment settings. Limiting such exposure would curtail respiratory diseases, such as farmer's lung and COPD, and may contribute to overall workplace well-being. As noted in the review, the use of such instrumentation in hospitals could greatly aid immune compromised patients by identifying particular practices that may generate PBAP levels that are harmful to those with respiratory ailments. Such information could then form the basis of PBAP abatement strategies within the aforementioned settings. Overall, it is hoped that the more wide-scale use of these instruments will provide governments, industry, and the scientific community even greater scope to monitor and assess the impact of PBAP on health and climate related factors.

Acknowledgments: The authors acknowledge funding received from the healthcare infection society (major research grant MPR/2015_07/012).

Author Contributions: All authors contributed to the researching and writing of the paper.

Conflicts of Interest: The authors declare no conflict of interest.

References

1. Seinfeld, J.H.; Pandis, S.N. *Atmospheric Chemistry and Physics: From Air Pollution to Climate Change*; Wiley: Hoboken, NJ, USA, 2016.
2. Zhu, Y.; Hinds, W.C.; Kim, S.; Shen, S.; Sioutas, C. Study of ultrafine particles near a major highway with heavy-duty diesel traffic. *Atmos. Environ.* **2002**, *36*, 4323–4335. [CrossRef]
3. Després, V.R.; Huffman, J.A.; Burrows, S.M.; Hoose, C.; Safatov, A.S.; Buryak, G.; Fröhlich-Nowoisky, J.; Elbert, W.; Andreae, M.O.; Pöschl, U. Primary biological aerosol particles in the atmosphere: A review. *Tellus B* **2012**, *64*. [CrossRef]
4. Douwes, J.; Thorne, P.; Pearce, N.; Heederik, D. Bioaerosol health effects and exposure assessment: Progress and prospects. *Ann. Occup. Hyg.* **2003**, *47*, 187–200. [PubMed]
5. Séguin, V.; Lemauviel-Lavenant, S.; Garon, D.; Bouchart, V.; Gallard, Y.; Blanchet, B.; Diquelou, S.; Personeni, E.; Gauduchon, P.; Ourry, A. Effect of agricultural and environmental factors on the hay characteristics involved in equine respiratory disease. *Agric. Ecosyst. Environ.* **2010**, *135*, 206–215. [CrossRef]
6. Sorenson, W.G. Fungal spores: Hazardous to health? *Environ. Health Perspect.* **1999**, *107*, 469–472. [CrossRef] [PubMed]
7. Peraica, M.; Radic, B.; Lucic, A.; Pavlovic, M. Toxic effects of mycotoxins in humans. *Bull. World Health Organ.* **1999**, *77*, 754–766. [PubMed]
8. Pope, C.A., III; Burnett, R.T.; Thun, M.J.; Calle, E.E.; Krewski, D.; Ito, K.; Thurston, G.D. Lung cancer, cardiopulmonary mortality, and long-term exposure to fine particulate air pollution. *JAMA* **2002**, *287*, 1132–1141. [CrossRef] [PubMed]
9. Jerrett, M.; Burnett, R.T.; Pope, C.A., 3rd; Ito, K.; Thurston, G.; Krewski, D.; Shi, Y.; Calle, E.; Thun, M. Long-term ozone exposure and mortality. *N. Engl. J. Med.* **2009**, *360*, 1085–1095.

10. Künzli, N.; Kaiser, R.; Medina, S.; Studnicka, M.; Chanel, O.; Filliger, P.; Herry, M.; Horak, F.; Puybonnieux-Texier, V.; Quénel, P. Public-health impact of outdoor and traffic-related air pollution: A European assessment. *Lancet* **2000**, *356*, 795–801. [CrossRef]
11. Fenger, J. Urban air quality. *Atmos. Environ.* **1999**, *33*, 4877–4900. [CrossRef]
12. Haga, D.I.; Burrows, S.M.; Iannone, R.; Wheeler, M.J.; Mason, R.H.; Chen, J.; Polishchuk, E.A.; Pöschl, U.; Bertram, A.K. Ice nucleation by fungal spores from the classes agaricomycetes, ustilaginomycetes, and eurotiomycetes, and the effect on the atmospheric transport of these spores. *Atmos. Chem. Phys.* **2014**, *14*, 8611–8630. [CrossRef]
13. Rogers, D.C.; DeMott, P.J.; Kreidenweis, S.M.; Chen, Y. Measurements of ice nucleating aerosols during SUCCESS. *Geophys. Res. Lett.* **1998**, *25*, 1383–1386. [CrossRef]
14. Mason, R.; Si, M.; Li, J.; Chou, C.; Dickie, R.; Toom-Sauntry, D.; Pöhlker, C.; Yakobi-Hancock, J.; Ladino, L.; Jones, K. Ice nucleating particles at a coastal marine boundary layer site: Correlations with aerosol type and meteorological conditions. *Atmos. Chem. Phys.* **2015**, *15*, 12547–12566. [CrossRef]
15. Hoose, C.; Kristjánsson, J.; Burrows, S. How important is biological ice nucleation in clouds on a global scale? *Environ. Res. Lett.* **2010**, *5*, 24009. [CrossRef]
16. Hummel, M.; Hoose, C.; Gallagher, M.; Healy, D.; Huffman, J.; O'Connor, D.; Pöschl, U.; Pöhlker, C.; Robinson, N.; Schnaiter, M. Regional-scale simulations of fungal spore aerosols using an emission parameterization adapted to local measurements of fluorescent biological aerosol particles. *Atmos. Chem. Phys.* **2015**, *15*, 6127–6146. [CrossRef]
17. O'Gorman, C.M.; Fuller, H.T. Prevalence of culturable airborne spores of selected allergenic and pathogenic fungi in outdoor air. *Atmos. Environ.* **2008**, *42*, 4355–4368. [CrossRef]
18. O'Connor, D.J.; Sadyś, M.; Skjøth, C.A.; Healy, D.A.; Kennedy, R.; Sodeau, J.R. Atmospheric concentrations of Alternaria, Cladosporium, Ganoderma and Didymella spores monitored in Cork (Ireland) and Worcester (England) during the summer of 2010. *Aerobiologia* **2014**, *30*, 397–411. [CrossRef]
19. Skjøth, C.A.; Sommer, J.; Stach, A.; Smith, M.; Brandt, J. The long-range transport of birch (Betula) pollen from Poland and Germany causes significant pre-season concentrations in Denmark. *Clin. Exp. Allergy* **2007**, *37*, 1204–1212. [CrossRef] [PubMed]
20. Galán, C.; Alcázar, P.; Cariñanos, P.; Garcia, H.; Domínguez-Vilches, E. Meteorological factors affecting daily Urticaceae pollen counts in southwest Spain. *Int. J. Biometeorol.* **2000**, *43*, 191–195. [CrossRef] [PubMed]
21. Gabey, A.; Stanley, W.; Gallagher, M.; Kaye, P.H. The fluorescence properties of aerosol larger than 0.8 μm in urban and tropical rainforest locations. *Atmos. Chem. Phys.* **2011**, *11*, 5491–5504. [CrossRef]
22. O'Connor, D.; Healy, D.; Sodeau, J. A 1-month online monitoring campaign of ambient fungal spore concentrations in the harbour region of Cork, Ireland. *Aerobiologia* **2015**, *31*, 295–314. [CrossRef]
23. Huffman, J.; Treutlein, B.; Pöschl, U. Fluorescent biological aerosol particle concentrations and size distributions measured with an Ultraviolet Aerodynamic Particle Sizer (UV-APS) in Central Europe. *Atmos. Chem. Phys.* **2010**, *10*, 3215–3233. [CrossRef]
24. Pöhlker, C.; Huffman, J.; Poschl, U. Autofluorescence of atmospheric bioaerosols-fluorescent biomolecules and potential interferences. *Atmos. Meas. Tech.* **2012**, *5*, 37–71. [CrossRef]
25. Pöhlker, C.; Huffman, J.A.; Förster, J.-D.; Pöschl, U. Autofluorescence of atmospheric bioaerosols: Spectral fingerprints and taxonomic trends of pollen. *Atmos. Meas. Tech.* **2013**, *6*, 3369–3392. [CrossRef]
26. Roshchina, V.V. *Fluorescing World of Plant Secreting Cells*; Science Publishers: New York, NY, USA, 2008.
27. Weber, G.; Teale, F. Determination of the absolute quantum yield of fluorescent solutions. *Trans. Faraday Soc.* **1957**, *53*, 646–655. [CrossRef]
28. Kunit, M.; Puxbaum, H. Enzymatic determination of the cellulose content of atmospheric aerosols. *Atmos. Environ.* **1996**, *30*, 1233–1236. [CrossRef]
29. Winiwarter, W.; Bauer, H.; Caseiro, A.; Puxbaum, H. Quantifying emissions of primary biological aerosol particle mass in Europe. *Atmos. Environ.* **2009**, *43*, 1403–1409. [CrossRef]
30. Mel'nikova, Y.V.; Roshchina, V.; Karnaukhov, V. Microspectrofluorimetry of intact plant pollen. *Biophysics* **1997**, *1*, 243–251.
31. O'Connor, D.J.; Iacopino, D.; Healy, D.A.; O'Sullivan, D.; Sodeau, J.R. The intrinsic fluorescence spectra of selected pollen and fungal spores. *Atmos. Environ.* **2011**, *45*, 6451–6458. [CrossRef]

32. O'Connor, D.J.; Healy, D.A.; Hellebust, S.; Buters, J.T.; Sodeau, J.R. Using the WIBS-4 (Waveband Integrated Bioaerosol Sensor) Technique for the On-Line Detection of Pollen Grains. *Aerosol Sci. Technol.* **2014**, *48*, 341–349. [CrossRef]
33. Jabaji-Hare, S.; Perumalla, C.; Kendrick, W. Autofluorescence of vesicles, arbuscules, and intercellular hyphae of a vesicular–arbuscular fungus in leek (Allium porrum) roots. *Can. J. Bot.* **1984**, *62*, 2665–2669. [CrossRef]
34. Albinsson, B.; Li, S.; Lundquist, K.; Stomberg, R. The origin of lignin fluorescence. *J. Mol. Struct.* **1999**, *508*, 19–27. [CrossRef]
35. Kozioł, J.; Knobloch, E. The solvent effect on the fluorescence and light absorption of riboflavin and lumiflavin. *Biochim. Biophys. Acta (BBA)-Biophys. Incl. Photosynth.* **1965**, *102*, 289–300.
36. O'Connor, D.J.; Lovera, P.; Iacopino, D.; O'Riordan, A.; Healy, D.A.; Sodeau, J.R. Using spectral analysis and fluorescence lifetimes to discriminate between grass and tree pollen for aerobiological applications. *Anal. Methods* **2014**, *6*, 1633–1639. [CrossRef]
37. Pisarevskii, A.; Cherenkevich, S.; Andrianov, V. Fluorescence spectrum and quantum yield of DNA in solution. *J. Appl. Spectrosc.* **1966**, *5*, 452–454. [CrossRef]
38. Morgan, J.P.; Daniels, M. Excited states of DNA and its components at room temperature—III. Spectra, polarisation and quantum yields of emissions from ApA and poly rA. *Photochem. Photobiol.* **1980**, *31*, 101–113. [CrossRef]
39. Lakowicz, J.R.; Shen, B.; Gryczynski, Z.; D'Auria, S.; Gryczynski, I. Intrinsic fluorescence from DNA can be enhanced by metallic particles. *Biochem. Biophys. Res. Commun.* **2001**, *286*, 875–879. [CrossRef] [PubMed]
40. Roshchina, V.; Mel'nikova, E.; Kovaleva, L. Changes in fluorescence during development of the male gametophyte. *Russ. J. Plant Physiol.* **1997**, *44*, 36–44.
41. Saxena, P. *Chemistry of Alkaloids*; Discovery Publishing House: New Delhi, India, 2007.
42. Coble, P.G. Characterization of marine and terrestrial DOM in seawater using excitation-emission matrix spectroscopy. *Mar. Chem.* **1996**, *51*, 325–346. [CrossRef]
43. Hudson, N.; Baker, A.; Reynolds, D. Fluorescence analysis of dissolved organic matter in natural, waste and polluted waters—A review. *River Res. Appl.* **2007**, *23*, 631–649. [CrossRef]
44. Muller, C.L.; Baker, A.; Hutchinson, R.; Fairchild, I.J.; Kidd, C. Analysis of rainwater dissolved organic carbon compounds using fluorescence spectrophotometry. *Atmos. Environ.* **2008**, *42*, 8036–8045. [CrossRef]
45. Bones, D.L.; Henricksen, D.K.; Mang, S.A.; Gonsior, M.; Bateman, A.P.; Nguyen, T.B.; Cooper, W.J.; Nizkorodov, S.A. Appearance of strong absorbers and fluorophores in limonene-O3 secondary organic aerosol due to NH4+-mediated chemical aging over long time scales. *J. Geophys. Res. Atmos.* **2010**, *115*. [CrossRef]
46. Monks, P.; Granier, C.; Fuzzi, S.; Stohl, A.; Williams, M.; Akimoto, H.; Amann, M.; Baklanov, A.; Baltensperger, U.; Bey, I. Atmospheric composition change–global and regional air quality. *Atmos. Environ.* **2009**, *43*, 5268–5350. [CrossRef]
47. Gillette, D.A.; Walker, T.R. Characteristics of airborne particles produced by wind erosion of sandy soil, High Plains of west Texas. *Soil Sci.* **1977**, *123*, 97–110. [CrossRef]
48. Andreae, M.; Rosenfeld, D. Aerosol–cloud–precipitation interactions. Part 1. The nature and sources of cloud-active aerosols. *Earth-Sci. Rev.* **2008**, *89*, 13–41. [CrossRef]
49. Bozlee, B.J.; Misra, A.K.; Sharma, S.K.; Ingram, M. Remote Raman and fluorescence studies of mineral samples. *Spectrochim. Acta Part A* **2005**, *61*, 2342–2348. [CrossRef] [PubMed]
50. Finlayson-Pitts, B.J.; Pitts, J.N., Jr. *Chemistry of the Upper and Lower Atmosphere: Theory, Experiments, and Applications*; Academic Press: Waltham, MA, USA, 1999.
51. Slowik, J.G.; Cross, E.S.; Han, J.-H.; Kolucki, J.; Davidovits, P.; Williams, L.R.; Onasch, T.B.; Jayne, J.T.; Kolb, C.E.; Worsnop, D.R. Measurements of morphology changes of fractal soot particles using coating and denuding experiments: Implications for optical absorption and atmospheric lifetime. *Aerosol Sci. Technol.* **2007**, *41*, 734–750. [CrossRef]
52. Kumke, M.; Löhmannsröben, H.-G.; Roch, T. Fluorescence spectroscopy of polynuclear aromatic compounds in environmental monitoring. *J. Fluoresc.* **1995**, *5*, 139–152. [CrossRef] [PubMed]
53. Lewitzka, F.; Niessner, R. Application of time-resolved fluorescence spectroscopy on the analysis of PAH-coated aerosols. *Aerosol Sci. Technol.* **1995**, *23*, 454–464. [CrossRef]

54. Panne, U.; Knöller, A.; Kotzick, R.; Niessner, R. On-line and in-situ detection of polycyclic aromatic hydrocarbons (PAH) on aerosols via thermodesorption and laser-induced fluorescence spectroscopy. *Fresenius J. Anal. Chem.* **2000**, *366*, 408–414. [CrossRef] [PubMed]
55. Savage, N.; Krentz, C.; Könemann, T.; Han, T.T.; Mainelis, G.; Pöhlker, C.; Huffman, J.A. Systematic Characterization and Fluorescence Threshold Strategies for the Wideband Integrated Bioaerosol Sensor (WIBS) Using Size-Resolved Biological and Interfering Particles. *Atmos. Meas. Tech.* **2017**, *10*, 4279–4302. [CrossRef]
56. Hairston, P.P.; Ho, J.; Quant, F.R. Design of an instrument for real-time detection of bioaerosols using simultaneous measurement of particle aerodynamic size and intrinsic fluorescence. *J. Aerosol Sci.* **1997**, *28*, 471–482. [CrossRef]
57. Huffman, J.; Sinha, B.; Garland, R.; Snee-Pollmann, A.; Gunthe, S.; Artaxo, P.; Martin, S.; Andreae, M.; Pöschl, U. Size distributions and temporal variations of biological aerosol particles in the Amazon rainforest characterized by microscopy and real-time UV-APS fluorescence techniques during AMAZE-08. *Atmos. Chem. Phys.* **2012**, *12*, 11997–12019. [CrossRef]
58. Morawska, L.; Johnson, G.; Ristovski, Z.; Hargreaves, M.; Mengersen, K.; Chao, C.; Wan, M.P.; Li, Y.; Xie, X.; Katoshevski, D. Droplets expelled during human expiratory activities and their origin. In Proceedings of the International Conference on Indoor Air Quality and Climate, Copenhagen, Denmark, 17–22 August 2008.
59. Brosseau, L.M.; Vesley, D.; Rice, N.; Goodell, K.; Nellis, M.; Hairston, P. Differences in detected fluorescence among several bacterial species measured with a direct-reading particle sizer and fluorescence detector. *Aerosol Sci. Technol.* **2000**, *32*, 545–558. [CrossRef]
60. Kulkarni, P.; Baron, P.A.; Willeke, K. *Aerosol Measurement: Principles, Techniques, and Applications*; Wiley: Hoboken, NJ, USA, 2011.
61. Kanaani, H.; Hargreaves, M.; Ristovski, Z.; Morawska, L. Performance assessment of UVAPS: Influence of fungal spore age and air exposure. *J. Aerosol Sci.* **2007**, *38*, 83–96. [CrossRef]
62. Agranovski, V.; Ristovski, Z.D.; Ayoko, G.A.; Morawska, L. Performance evaluation of the UVAPS in measuring biological aerosols: Fluorescence spectra from NAD (P) H coenzymes and riboflavin. *Aerosol Sci. Technol.* **2004**, *38*, 354–364. [CrossRef]
63. Knibbs, L.D.; He, C.; Duchaine, C.; Morawska, L. Vacuum cleaner emissions as a source of indoor exposure to airborne particles and bacteria. *Environ. Sci. Technol.* **2011**, *46*, 534–542. [CrossRef] [PubMed]
64. Jung, J.H.; Lee, J.E.; Hwang, G.B.; Lee, B.U.; Lee, S.B.; Jurng, J.S.; Bae, G.N. Electrospray-assisted ultraviolet aerodynamic particle sizer spectrometer for real-time characterization of bacterial particles. *Anal. Chem.* **2009**, *82*, 664–671. [CrossRef] [PubMed]
65. Johnson, G.R.; Morawska, L. The mechanism of breath aerosol formation. *J. Aerosol Med. Pulm. Drug Deliv.* **2009**, *22*, 229–237. [CrossRef] [PubMed]
66. Perrott, P.; Hargreaves, M. Detection of Bacteriophage in Droplets. In *Human Respiratory Syncytial Virus Infection*; InTech: Lexington, KY, USA, 2011.
67. Agranovski, V.; Ristovski, Z.; Hargreaves, M.; Blackall, P.J.; Morawska, L. Performance evaluation of the UVAPS: Influence of physiological age of airborne bacteria and bacterial stress. *J. Aerosol Sci.* **2003**, *34*, 1711–1727. [CrossRef]
68. Kaliszewski, M.; Trafny, E.A.; Lewandowski, R.; Włodarski, M.; Bombalska, A.; Kopczyński, K.; Antos-Bielska, M.; Szpakowska, M.; Młyńczak, J.; Mularczyk-Oliwa, M.; et al. A new approach to UVAPS data analysis towards detection of biological aerosol. *J. Aerosol Sci.* **2013**, *58*, 148–157. [CrossRef]
69. Ratnesar-Shumate, S.; Wagner, M.L.; Kerechanin, C.; House, G.; Brinkley, K.M.; Bare, C.; Baker, N.A.; Quizon, R.; Quizon, J.; Proescher, A. Improved method for the evaluation of real-time biological aerosol detection technologies. *Aerosol Sci. Technol.* **2011**, *45*, 635–644. [CrossRef]
70. Zheng, Y.; Yao, M. Liquid impinger BioSampler's performance for size-resolved viable bioaerosol particles. *J. Aerosol Sci.* **2017**, *106*, 34–42. [CrossRef]
71. Ratnesar-Shumate, S.; Pan, Y.-L.; Hill, S.C.; Kinahan, S.; Corson, E.; Eshbaugh, J.; Santarpia, J.L. Fluorescence spectra and biological activity of aerosolized bacillus spores and MS2 bacteriophage exposed to ozone at different relative humidities in a rotating drum. *J. Quant. Spectrosc. Radiat. Transf.* **2015**, *153*, 13–28. [CrossRef]
72. Zou, Z.; Yao, M. Airflow resistance and bio-filtering performance of carbon nanotube filters and current facepiece respirators. *J. Aerosol Sci.* **2015**, *79*, 61–71. [CrossRef]

73. Santarpia, J.L.; Pan, Y.-L.; Hill, S.C.; Baker, N.; Cottrell, B.; McKee, L.; Ratnesar-Shumate, S.; Pinnick, R.G. Changes in fluorescence spectra of bioaerosols exposed to ozone in a laboratory reaction chamber to simulate atmospheric aging. *Opt. Express* **2012**, *20*, 29867–29881. [CrossRef] [PubMed]
74. Pan, Y.-L.; Santarpia, J.L.; Ratnesar-Shumate, S.; Corson, E.; Eshbaugh, J.; Hill, S.C.; Williamson, C.C.; Coleman, M.; Bare, C.; Kinahan, S. Effects of ozone and relative humidity on fluorescence spectra of octapeptide bioaerosol particles. *J. Quant. Spectrosc. Radiat. Transf.* **2014**, *133*, 538–550. [CrossRef]
75. Bhangar, S.; Adams, R.I.; Pasut, W.; Huffman, J.; Arens, E.A.; Taylor, J.W.; Bruns, T.D.; Nazaroff, W.W. Chamber bioaerosol study: Human emissions of size-resolved fluorescent biological aerosol particles. *Indoor Air* **2016**, *26*, 193–206. [CrossRef] [PubMed]
76. Park, C.W.; Yoon, K.Y.; Byeon, J.H.; Kim, K.; Hwang, J. Development of rapid assessment method to determine bacterial viability based on ultraviolet and visible (UV-Vis) spectroscopy analysis including application to bioaerosols. *Aerosol Air Qual. Res.* **2012**, *12*, 395–404. [CrossRef]
77. Saari, S.; Putkiranta, M.; Keskinen, J. Fluorescence spectroscopy of atmospherically relevant bacterial and fungal spores and potential interferences. *Atmos. Environ.* **2013**, *71*, 202–209. [CrossRef]
78. Kanaani, H.; Hargreaves, M.; Ristovski, Z.; Morawska, L. Deposition rates of fungal spores in indoor environments, factors effecting them and comparison with non-biological aerosols. *Atmos. Environ.* **2008**, *42*, 7141–7154. [CrossRef]
79. Cieślik, I.; Żmija, J.; Majchrowski, A.; Pępczyńska, M.; Morawiak, P.; Włodarski, M. Synthesis and characteristics of optical properties of crystalline $YAl_3(BO_3)_4$:Cr,Ce. *J. Achiev. Mater. Manuf. Eng.* **2011**, *48*, 24–28.
80. Cieślik, I.; Węgłowski, R.; Żmija, J.; Kurzydłowski, K.; Płocińska, M.; Oćwieja, M. Control of optical active borates nanocrystals agglomeration. *J. Achiev. Mater. Manuf. Eng.* **2013**, *61*, 163–168.
81. Agranovski, V.; Ristovski, Z.D. Real-time monitoring of viable bioaerosols: Capability of the UVAPS to predict the amount of individual microorganisms in aerosol particles. *J. Aerosol Sci.* **2005**, *36*, 665–676. [CrossRef]
82. Kanaani, H.; Hargreaves, M.; Smith, J.; Ristovski, Z.; Agranovski, V.; Morawska, L. Performance of UVAPS with respect to detection of airborne fungi. *J. Aerosol Sci.* **2008**, *39*, 175–189. [CrossRef]
83. Agranovski, V.; Ristovski, Z.; Hargreaves, M.; Blackall, P.J.; Morawska, L. Real-time measurement of bacterial aerosols with the UVAPS: Performance evaluation. *J. Aerosol Sci.* **2003**, *34*, 301–317. [CrossRef]
84. Roshchina, V.; Karnaukhov, V. Changes in pollen autofluorescence induced by ozone. *Biol. Plant.* **1999**, *42*, 273–278. [CrossRef]
85. Schumacher, C.; Pöhlker, C.; Aalto, P.; Hiltunen, V.; Petäjä, T.; Kulmala, M.; Pöschl, U.; Huffman, J. Seasonal cycles of fluorescent biological aerosol particles in boreal and semi-arid forests of Finland and Colorado. *Atmos. Chem. Phys.* **2013**, *13*, 11987–12001. [CrossRef]
86. Li, J.; Zhou, L.; Zhang, X.; Xu, C.; Dong, L.; Yao, M. Bioaerosol emissions and detection of airborne antibiotic resistance genes from a wastewater treatment plant. *Atmos. Environ.* **2016**, *124*, 404–412. [CrossRef]
87. Valsan, A.; Ravikrishna, R.; Biju, C.; Pöhlker, C.; Després, V.; Huffman, J.; Pöschl, U.; Gunthe, S. Fluorescent biological aerosol particle measurements at a tropical high-altitude site in southern India during the southwest monsoon season. *Atmos. Chem. Phys.* **2016**, *16*, 9805–9830. [CrossRef]
88. Pöschl, U.; Martin, S.; Sinha, B.; Chen, Q.; Gunthe, S.; Huffman, J.; Borrmann, S.; Farmer, D.; Garland, R.; Helas, G. Rainforest aerosols as biogenic nuclei of clouds and precipitation in the Amazon. *Science* **2010**, *329*, 1513–1516. [CrossRef] [PubMed]
89. Hallar, A.; Chirokova, G.; McCubbin, I.; Painter, T.H.; Wiedinmyer, C.; Dodson, C. Atmospheric bioaerosols transported via dust storms in the western United States. *Geophys. Res. Lett.* **2011**, *38*. [CrossRef]
90. Huffman, J.A.; Prenni, A.; DeMott, P.; Pöhlker, C.; Mason, R.; Robinson, N.; Fröhlich-Nowoisky, J.; Tobo, Y.; Després, V.; Garcia, E.; et al. High concentrations of biological aerosol particles and ice nuclei during and after rain. *Atmos. Chem. Phys.* **2013**, *13*, 6151–6164. [CrossRef]
91. Gosselin, M.I.; Rathnayake, C.M.; Crawford, I.; Pöhlker, C.; Fröhlich-Nowoisky, J.; Schmer, B.; Després, V.R.; Engling, G.; Gallagher, M.; Stone, E.; et al. Fluorescent bioaerosol particle, molecular tracer, and fungal spore concentrations during dry and rainy periods in a semi-arid forest. *Atmos. Chem. Phys.* **2016**, *16*, 15165–15184. [CrossRef]

92. Wei, K.; Zou, Z.; Zheng, Y.; Li, J.; Shen, F.; Wu, C.-Y.; Wu, Y.; Hu, M.; Yao, M. Ambient bioaerosol particle dynamics observed during haze and sunny days in Beijing. *Sci. Total Environ.* **2016**, *550*, 751–759. [CrossRef] [PubMed]
93. Fan, H.; Li, X.; Deng, J.; Da, G.; Gehin, E.; Yao, M. Time-dependent size-resolved bacterial and fungal aerosols in Beijing subway. *Aerosol Air Qual. Res.* **2016**, *10*, 1–11. [CrossRef]
94. Li, J.; Li, M.; Shen, F.; Zou, Z.; Yao, M.; Wu, C.-y. Characterization of biological aerosol exposure risks from automobile air conditioning system. *Environ. Sci. Technol.* **2013**, *47*, 10660–10666. [CrossRef] [PubMed]
95. Wei, K.; Zheng, Y.; Li, J.; Shen, F.; Zou, Z.; Fan, H.; Li, X.; Wu, C.-y.; Yao, M. Microbial aerosol characteristics in highly polluted and near-pristine environments featuring different climatic conditions. *Sci. Bull.* **2015**, *60*, 1439–1447. [CrossRef]
96. Saari, S.; Niemi, J.; Rönkkö, T.; Kuuluvainen, H.; Järvinen, A.; Pirjola, L.; Aurela, M.; Hillamo, R.; Keskinen, J. Seasonal and diurnal variations of fluorescent bioaerosol concentration and size distribution in the urban environment. *Aerosol Air Qual. Res.* **2015**, *15*, 572–581. [CrossRef]
97. Manninen, H.E.; Bäck, J.; Sihto-Nissilä, S.-L.; Huffman, J.A.; Pessi, A.-M.; Hiltunen, V.; Aalto, P.P.; Hidalgo Fernández, P.J.; Hari, P.; Saarto, A.; et al. Patterns in airborne pollen and other primary biological aerosol particles (PBAP), and their contribution to aerosol mass and number in a boreal forest. *Boreal Environ. Res.* **2014**, *19*, 383–405.
98. Healy, D.; Huffman, J.; O'Connor, D.; Pöhlker, C.; Pöschl, U.; Sodeau, J. Ambient measurements of biological aerosol particles near Killarney, Ireland: A comparison between real-time fluorescence and microscopy techniques. *Atmos. Chem. Phys.* **2014**, *14*, 8055–8069. [CrossRef]
99. O'Connor, D.J.; Healy, D.A.; Sodeau, J.R. The on-line detection of biological particle emissions from selected agricultural materials using the WIBS-4 (Waveband Integrated Bioaerosol Sensor) technique. *Atmos. Environ.* **2013**, *80*, 415–425. [CrossRef]
100. Hameed, A.A.; Khodr, M. Suspended particulates and bioaerosols emitted from an agricultural non-point source. *J. Environ. Monit.* **2001**, *3*, 206–209. [CrossRef] [PubMed]
101. Agranovski, V.; Ristovski, Z.; Blackall, P.J.; Morawska, L. Size-selective assessment of airborne particles in swine confinement building with the UVAPS. *Atmos. Environ.* **2004**, *38*, 3893–3901. [CrossRef]
102. Xu, C.; Wu, C.-Y.; Yao, M. Fluorescent Bioaerosol Particles Resulting from Human Occupancy with and without Respirators. *Aerosol Air Qual. Res.* **2017**, *17*, 198–208. [CrossRef]
103. Lavoie, J.; Marchand, G.; Cloutier, Y.; Hallé, S.; Nadeau, S.; Duchaine, C.; Pichette, G. Evaluation of bioaerosol exposures during hospital bronchoscopy examinations. *Environ. Sci.* **2015**, *17*, 288–299. [CrossRef] [PubMed]
104. Bhangar, S.; Huffman, J.; Nazaroff, W. Size-resolved fluorescent biological aerosol particle concentrations and occupant emissions in a university classroom. *Indoor Air* **2014**, *24*, 604–617. [CrossRef] [PubMed]
105. Pereira, M.L.; Knibbs, L.D.; He, C.; Grzybowski, P.; Johnson, G.R.; Huffman, J.A.; Bell, S.C.; Wainwright, C.E.; Matte, D.L.; Dominski, F.H. Sources and dynamics of fluorescent particles in hospitals. *Indoor Air* **2017**, *27*, 988–1000. [CrossRef] [PubMed]
106. He, C.; Salonen, H.; Ling, X.; Crilley, L.; Jayasundara, N.; Cheung, H.C.; Hargreaves, M.; Huygens, F.; Knibbs, L.D.; Ayoko, G.A. The impact of flood and post-flood cleaning on airborne microbiological and particle contamination in residential houses. *Environ. Int.* **2014**, *69*, 9–17. [CrossRef] [PubMed]
107. Prenni, A.; Tobo, Y.; Garcia, E.; DeMott, P.; Huffman, J.; McCluskey, C.; Kreidenweis, S.; Prenni, J.; Pöhlker, C.; Pöschl, U. The impact of rain on ice nuclei populations at a forested site in Colorado. *Geophys. Res. Lett.* **2013**, *40*, 227–231. [CrossRef]
108. Kaye, P.H.; Stanley, W.R.; Foot, E.V.J. Fluid-Borne Particle Detector. Google Patents US8711353 B2, 29 April 2014.
109. Technologies, D.M. *Wideband Integrated Bioaerosol Sensor (WIBS-4a) Operator Manual*; Droplet Measurement Technologies: Longmont, CO, USA, 2014.
110. Healy, D.A.; O'Connor, D.J.; Burke, A.M.; Sodeau, J.R. A laboratory assessment of the Waveband Integrated Bioaerosol Sensor (WIBS-4) using individual samples of pollen and fungal spore material. *Atmos. Environ.* **2012**, *60*, 534–543. [CrossRef]
111. Stanley, W.R.; Kaye, P.H.; Foot, V.E.; Barrington, S.J.; Gallagher, M.; Gabey, A. Continuous bioaerosol monitoring in a tropical environment using a UV fluorescence particle spectrometer. *Atmos. Sci. Lett.* **2011**, *12*, 195–199. [CrossRef]

112. Gabey, A.; Gallagher, M.; Whitehead, J.; Dorsey, J.; Kaye, P.H.; Stanley, W. Measurements and comparison of primary biological aerosol above and below a tropical forest canopy using a dual channel fluorescence spectrometer. *Atmos. Chem. Phys.* **2010**, *10*, 4453–4466. [CrossRef]
113. Perring, A.; Schwarz, J.; Baumgardner, D.; Hernandez, M.; Spracklen, D.; Heald, C.; Gao, R.; Kok, G.; McMeeking, G.; McQuaid, J. Airborne observations of regional variation in fluorescent aerosol across the United States. *J. Geophys. Res. Atmos.* **2015**, *120*, 1153–1170. [CrossRef]
114. Robinson, N.H.; Allan, J.; Huffman, J.; Kaye, P.H.; Foot, V.; Gallagher, M. Cluster analysis of WIBS single-particle bioaerosol data. *Atmos. Meas. Tech.* **2013**, *6*, 337–347. [CrossRef]
115. Healy, D.A.; O'Connor, D.J.; Sodeau, J.R. Measurement of the particle counting efficiency of the "Waveband Integrated Bioaerosol Sensor" model number 4 (WIBS-4). *J. Aerosol Sci.* **2012**, *47*, 94–99. [CrossRef]
116. Toprak, E.; Schnaiter, M. Fluorescent biological aerosol particles measured with the Waveband Integrated Bioaerosol Sensor WIBS-4: Laboratory tests combined with a one year field study. *Atmos. Chem. Phys.* **2013**, *13*, 225–243. [CrossRef]
117. Hernandez, M.; Perring, A.E.; McCabe, K.; Kok, G.; Granger, G.; Baumgardner, D. Chamber catalogues of optical and fluorescent signatures distinguish bioaerosol classes. *Atmos. Meas. Tech.* **2016**, *9*, 3283–3292. [CrossRef]
118. Zhou, J.; Fang, W.; Cao, Q.; Yang, L.; Chang, V.C.; Nazaroff, W.W. Influence of moisturizer and relative humidity on human emissions of fluorescent biological aerosol particles. *Indoor Air* **2017**, *27*, 587–598. [CrossRef] [PubMed]
119. Robinson, E.S.; Gao, R.-S.; Schwarz, J.P.; Fahey, D.W.; Perring, A.E. Fluorescence calibration method for single-particle aerosol fluorescence instruments. *Atmos. Meas. Tech.* **2017**, *10*, 1755–1768. [CrossRef]
120. Gabey, A.; Vaitilingom, M.; Freney, E.; Boulon, J.; Sellegri, K.; Gallagher, M.; Crawford, I.; Robinson, N.; Stanley, W.; Kaye, P.H. Observations of fluorescent and biological aerosol at a high-altitude site in central France. *Atmos. Chem. Phys.* **2013**, *13*, 7415–7428. [CrossRef]
121. Crawford, I.; Robinson, N.; Flynn, M.; Foot, V.; Gallagher, M.; Huffman, J.; Stanley, W.; Kaye, P.H. Characterisation of bioaerosol emissions from a Colorado pine forest: Results from the BEACHON-RoMBAS experiment. *Atmos. Chem. Phys.* **2014**, *14*, 8559–8578. [CrossRef]
122. Yu, X.; Wang, Z.; Zhang, M.; Kuhn, U.; Xie, Z.; Cheng, Y.; Pöschl, U.; Su, H. Ambient measurement of fluorescent aerosol particles with a WIBS in the Yangtze River Delta of China: Potential impacts of combustion-related aerosol particles. *Atmos. Chem. Phys.* **2016**, *16*, 11337–11348. [CrossRef]
123. Xie, Y.; Fajardo, O.A.; Yan, W.; Zhao, B.; Jiang, J. Six-day measurement of size-resolved indoor fluorescent bioaerosols of outdoor origin in an office. *Particuology* **2017**, *31*, 161–169. [CrossRef]
124. Möhler, O.; DeMott, P.; Vali, G.; Levin, Z. Microbiology and atmospheric processes: The role of biological particles in cloud physics. *Biogeosciences* **2007**, *4*, 1059–1071. [CrossRef]
125. Prenni, A.J.; DeMott, P.J.; Kreidenweis, S.M.; Harrington, J.Y.; Avramov, A.; Verlinde, J.; Tjernström, M.; Long, C.N.; Olsson, P.Q. Can ice-nucleating aerosols affect Arctic seasonal climate? *Bull. Am. Meteorol. Soc.* **2007**, *88*, 541–550. [CrossRef]
126. Prenni, A.J.; Petters, M.D.; Kreidenweis, S.M.; Heald, C.L.; Martin, S.T.; Artaxo, P.; Garland, R.M.; Wollny, A.G.; Pöschl, U. Relative roles of biogenic emissions and Saharan dust as ice nuclei in the Amazon basin. *Nat. Geosci.* **2009**, *2*, 402–405. [CrossRef]
127. Twohy, C.H.; McMeeking, G.R.; DeMott, P.J.; McCluskey, C.S.; Hill, T.C.; Burrows, S.M.; Kulkarni, G.R.; Tanarhte, M.; Kafle, D.N.; Toohey, D.W. Abundance of fluorescent biological aerosol particles at temperatures conducive to the formation of mixed-phase and cirrus clouds. *Atmos. Chem. Phys.* **2016**, *16*, 8205–8225. [CrossRef]
128. Tobo, Y.; Prenni, A.J.; DeMott, P.J.; Huffman, J.A.; McCluskey, C.S.; Tian, G.; Pöhlker, C.; Pöschl, U.; Kreidenweis, S.M. Biological aerosol particles as a key determinant of ice nuclei populations in a forest ecosystem. *J. Geophys. Res. Atmos.* **2013**, *118*, 10100–10110. [CrossRef]
129. O'Connor, D.J.; Daly, S.M.; Sodeau, J.R. On-line monitoring of airborne bioaerosols released from a composting/green waste site. *Waste Manag.* **2015**, *42*, 23–30. [CrossRef] [PubMed]
130. Crawford, I.; Lloyd, G.; Herrmann, E.; Hoyle, C.; Bower, K.; Connolly, P.; Flynn, M.; Kaye, P.; Choularton, T.; Gallagher, M. Observations of fluorescent aerosol–cloud interactions in the free troposphere at the High-Altitude Research Station Jungfraujoch. *Atmos. Chem. Phys.* **2016**, *16*, 2273–2284. [CrossRef]

131. Wright, T.P.; Hader, J.D.; McMeeking, G.R.; Petters, M.D. High relative humidity as a trigger for widespread release of ice nuclei. *Aerosol Sci. Technol.* **2014**, *48*, i–v. [CrossRef]
132. Yue, S.; Ren, H.; Fan, S.; Wei, L.; Zhao, J.; Bao, M.; Hou, S.; Zhan, J.; Zhao, W.; Ren, L.; et al. High Abundance of Fluorescent Biological Aerosol Particles in Winter Beijing, China. *ACS Earth Space Chem.* **2017**, *1*, 493–502. [CrossRef]
133. Saari, S.; Reponen, T.; Keskinen, J. Performance of two fluorescence-based real-time bioaerosol detectors: BioScout vs. *UVAPS*. *Aerosol Sci. Technol.* **2013**, *48*, 371–378. [CrossRef]
134. Saari, S.; Mensah-Attipoe, J.; Reponen, T.; Veijalainen, A.; Salmela, A.; Pasanen, P.; Keskinen, J. Effects of fungal species, cultivation time, growth substrate, and air exposure velocity on the fluorescence properties of airborne fungal spores. *Indoor Air* **2015**, *25*, 653–661. [CrossRef] [PubMed]
135. Liu, M.; Huang, Y.; Ma, Z.; Jin, Z.; Liu, X.; Wang, H.; Liu, Y.; Wang, J.; Jantunen, M.; Bi, J. Spatial and temporal trends in the mortality burden of air pollution in China: 2004–2012. *Environ. Int.* **2017**, *98*, 75–81. [CrossRef] [PubMed]
136. Kiselev, D.; Bonacina, L.; Wolf, J.-P. Individual bioaerosol particle discrimination by multi-photon excited fluorescence. *Opt. Express* **2011**, *19*, 24516–24521. [CrossRef] [PubMed]
137. Kiselev, D.; Bonacina, L.; Wolf, J.-P. A flash-lamp based device for fluorescence detection and identification of individual pollen grains. *Rev. Sci. Instrum.* **2013**, *84*, 33302. [CrossRef] [PubMed]
138. Crouzy, B.; Stella, M.; Konzelmann, T.; Calpini, B.; Clot, B. All-optical automatic pollen identification: Towards an operational system. *Atmos. Environ.* **2016**, *140*, 202–212. [CrossRef]
139. Ruske, S.; Topping, D.O.; Foot, V.E.; Kaye, P.H.; Stanley, W.R.; Crawford, I.; Morse, A.P.; Gallagher, M.W. Evaluation of machine learning algorithms for classification of primary biological aerosol using a new UV-LIF spectrometer. *Atmos. Meas. Tech.* **2017**, *10*, 695–708. [CrossRef]